1

From Mechanochemistry to Mechanoresponsive Materials

Lasith S. Kariyawasam, Connor Filbin, Cameron Locke, and Ying Yang

University of Nevada, Department of Chemistry, Virginia Street, Reno, NV 89557, USA

1.1 Introduction

Our skin can sense the touch by a series of mechanotransduction mechanisms. Kneading bread dough uncoils gluten proteins, creating an elastic macromolecular network that gives the dough toughness. Stretching or scratching a piece of plastic is likely to break covalent bonds. These processes involve reactions that are activated by mechanical energy, which are prevalent in our daily lives. However, they are less commonly discussed compared to thermochemical, photochemical, or electrochemical reactions. Mechanoactivated reactions have been reported dating back to 315 BCE. These early accounts describe grinding native cinnabar in a copper mortar with a copper pestle in the presence of vinegar to yield the reduction product, mercury. However, it was not until the nineteenth century that systematic studies were conducted [1]. In 1860s, Carey Lea showed that grinding mercury and silver halides in a pestle and mortar at room temperature favors decomposition, whereas heating only leads to melting or sublimation without any decomposition [2]. This discovery provided clear evidence that mechanochemical reactions are distinctively different from thermal ones. Mechanochemistry was, therefore, classified as the fourth type of chemical reaction by Ostwald in 1919 [3].

The first widely accepted definition for mechanochemistry was formulated by Heinicke in 1984 [1], that mechanochemistry is a branch of chemistry, which is concerned with chemical and physicochemical transformations of substances in all states of aggregation produced by the effect of mechanical energy. IUPAC defines it as the chemical reaction that is induced by the direct absorption of mechanical energy [4]. In fact, the definition is still under extensive debate. Molecular motors, which convert chemical energy into mechanical work, certainly do not fit into these definitions. However, the motions generated by molecular motors can apply force to the surrounding molecules to induce a cascade of subsequent reactions. Such topic is of great interest to chemists and engineers working in the field of mechanochemistry. The lack of unification and slow progress since the establishment of mechanochemistry in the nineteenth century reflects the complexity and

Smart Stimuli-Responsive Polymers, Films, and Gels, First Edition.
Edited by Liang Hu, Yongfeng Gao, and Michael J. Serpe.

the lack of understanding of the scope and mechanisms for such reactions. Recently, mechanochemical research has intensified through the use of new tools developed for mechanistic studies and the opportunities to create functional materials [5–12]. As mechanochemical reactions occur for both small and macromolecules, ongoing research can be clarified in four sub-areas: developing novel and scalable mechanochemical synthesis to make useful chemicals via environmental-friendly solvent-free processes; understanding biomechanochemistry, such as motor proteins, mechanosensing, and mechanotransduction mechanisms; creating mechanoresponsive polymeric materials for which mechanical forces become constructive for technological advances; and investigating the molecular mechanisms through simulations and single-molecular force experiments.

In this chapter, we will focus on the fundamental aspects of polymer mechanochemistry that are the key elements in designing mechanoresponsive materials. We will start with a brief introduction of the role of mechanochemistry in biological systems as a springboard for inspiration. The mechanistic aspects of mechanochemistry in general terms, from small molecules to polymer mechanochemistry, will then be discussed to show the unique bond-activation mechanisms. The force-responsive molecules, named mechanophores, can depend on the cleavage of either covalent or noncovalent bonds. The activation energy, dynamics, and reversibility can be tuned via various structural properties. Therefore, the chemistry of these two classes of mechanophores will be covered in detail. There are different mechanical sources for generating mechanical energy, such as shearing, stretching, grinding, ball milling, and sonication. These methods differ in the direction of force, frequency, and heat formation, leading to different effects on molecular distortion and kinetics. However, this chapter will focus on the chemistry of mechanoresponsive bonds within polymer materials regardless of the type of applied force.

1.2 Mechanochemistry in Biological Systems

A powerful source of inspiration for improving the design of polymer materials is Nature as mechanochemical systems are ubiquitous in organisms. A wealth of knowledge can be gained because biological systems have evolved elegant mechanoresponsive arrangements that are critical for supporting and maintaining life. They often involve complicated processes via coherently organized biopolymer networks. A cell, for example, is constantly under mechanical stress, including tension, osmosis, compression, and shear forces. Upon mechanical deformation, feedback from proteins in the cell cytoskeleton activates a variety of mechanosensors that work in unison to create a response in the cell nucleus via multiple mechanotransduction events [13]. As shown in Figure 1.1, the mechanism begins by transducing force through the cell membrane to microfilaments and microtubules of the cytoskeleton in the cytoplasm. Subsequently, cytoskeletal changes directly affect nucleoskeletal proteins called lamina. This has an explicit effect on the spatial arrangement of lamin-bound intermediate filaments as well as

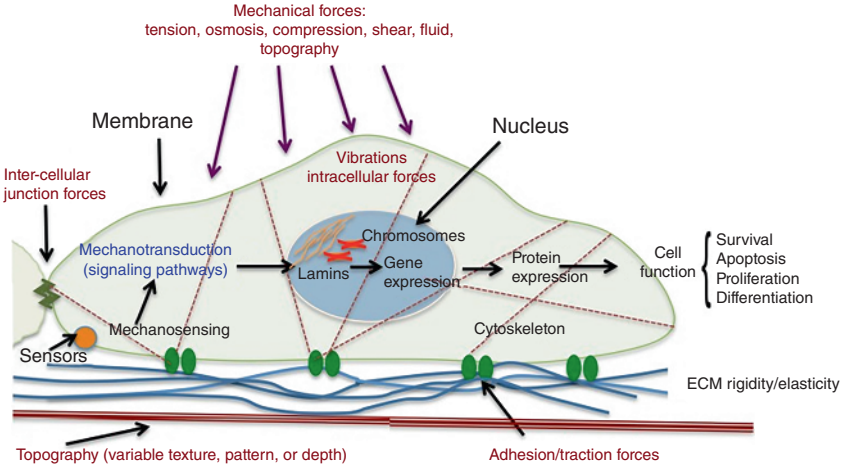

Figure 1.1 Intra- and extracellular forces stimulate a cell in an interconnected system of reactions causing complete change of structure and resulting cell function. Source: Adapted with permission from Tsimbouri [13]. Copyright 2015 MDPI.

chromosomes, as they are anchored to nuclear lamina [14]. Shifts in chromosome packing affect gene expression, which allows key biological functions in response to force, such as survival, motility, reproduction, and differentiation. These events in cells play important roles in maintaining homeostasis and preventing disease in the body. Although understanding of many of these biological pathways is still limited, we will discuss a few chemistries known to be involved in these processes as inspirations for material design.

1.2.1 A Stressful Environment During Heart Development

In a vertebrate embryo, the heart first starts as a tube composed of primarily early cardiomyocytes, the cardiac muscle cells that drive the heart contraction. It quickly differentiates into different parts and morphologies. As the embryo grows, the contractile capacity of the cardiomyocytes increases to provide greater driving forces to pump more blood. Meanwhile, the extracellular matrix (ECM) surrounding the cardiomyocytes must increase in its stiffness parallelly to keep a proper tissue mechanical integrity with the increasing contractile stress. Cells in connective tissue, called fibroblasts, secrete collagen and other matrix proteins to maintain the structural framework. Therefore, during the development of the heart, a balance between cardiac fibroblast and cardiomyocyte cell populations must be established to maintain muscle contraction along with a significant collagenous matrix. There is mounting evidence suggesting that mechanical stress itself plays important role in directing tissue growth with mechanochemical feedback loops for gene and protein expression [15]. In comparison, the brain tissue in a low-stress environment does not show the same development in stiffness, although a recent study found strong mechanical interactions of the synapses [16] which may be a critical mechanism in brain

functions, indicating the broad involvements of mechanochemistry and mechanotransduction in numerous bioprocesses.

During embryonic heart development, many mechanosensitive pathways have been linked to the proper functions of the myocyte and fibroblast cells. Majkut et al. surveyed literature evidence and proposed the network model for understanding how contraction against tissue stiffness affords a functional equilibrium between the cell types [15]. On one hand, cardiomyocytes produce contractile stress that promotes the expression of matrix structural proteins by fibroblasts. On the other hand, as contraction must effectively strain the heart tissue, it is postulated that the proliferation of fibroblasts is limited by the stiffness of their environment and thus collagenous matrix density. Additionally, the model suggests that stabilizing matrix collagen and degradation of motor proteins under strained conditions are also important in regulating tissue stiffness. The stabilization may be related to inhibited protease binding to collagen fibers or kinase binding to myosin minifilaments when they are under tension, thus preventing their dissociation and digestion. A model of dynamic cell–matrix interaction is also extended to nuclear mechanics because during development there are variations in lamin levels that appear to correlate with ECM mechanics [15]. As previously discussed, mechanical signals from the extracellular environment can be physically transmitted by the contractile cytoskeleton to the nucleus by connections through the nuclear membrane to the nuclear lamina. Lamina can interact with chromatin and various proteins that regulate transcription. Therefore, lamin expression is also regulated and affects tissue maturation.

1.2.2 Protein Unfolding by Force

Proteins are folded into various three-dimensional structures to perform biological functions. Many of them are highly resistant to unfolding under mechanical stress to avoid denaturation. However, it has been observed that certain proteins containing hidden binding sites (cryptic sites) that rely on force for a conformational change via unfolding to enable protein activity and initiation of signaling pathways [17–19]. One of the most extensively studied mechanically responsive proteins is the von Willebrand factor (vWF), which plays a crucial role in blood clotting. When vascular systems are ruptured, a decrease in pressure triggers hydrodynamic forces from changing velocity in the blood. These hydrodynamic forces induce a shear force on vWF in the blood, causing a conformation change. At a critical shear stress of approximately 50 dyn/cm^2, the globular protein is significantly elongated [20–22]. Figure 1.2 shows the domain structures and the force-induced conformational change. This leads to exposure and activation of the A1 domain to bind to platelets and A3 domain to attach to the collagen protein on the surface of vascular damage to initiate repair of the vessel injury [23]. The protein unfolding occurs at the A2 domain and is suggested to involve mechanoactivated cleavage of disulfide bonds in combination with hydrophobic interactions. The vWF contains an eight-membered ring linked by a disulfide bond from vicinal cysteines (Cys^{1669}–Cys^{1670}), which is the lowest energy barrier to initiate force-induced unfolding of the A2 domain

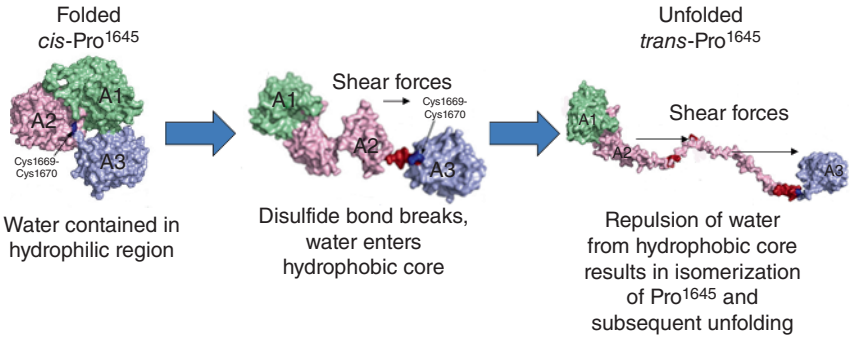

Figure 1.2 Model of vWF protein mechanochemical unfolding from shear forces. When vWF protein is in the unfolded conformation the A1 domain binds platelets (green), A2 domain elongates (pink), and A3 domain binds collagen (blue). Source: Adapted with permission from Crawleyet al. [21]. Copyright 2011 American Society of Hematology.

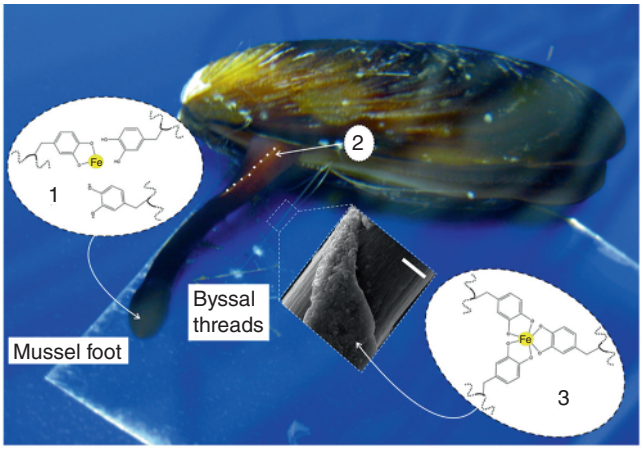

Figure 1.3 Schematic of marine mussel cuticle demonstrating high density of dopa-Fe^{3+} crosslinks in granule compared to matrix. This results in the formation of microcracks following increased strain, preventing complete material fracture. Source: Adapted with permission from Holten-Andersen et al. [24].

(Figure 1.3). When applied force is transduced through the protein, the disulfide bond is mechanically cleaved by shear forces. It is speculated that after cleavage, buried water molecules are admitted to the hydrophobic core of the vWF protein commencing unfolding [25]. Additionally, the unfolded state of the protein is stabilized by a force-induced isomerization of a proline residue (Pro^{1645}). The peptide *cis*-Pro^{1645} in the A2 domain is stabilized in a cis conformation by hydrogen bonding with residue Arg^{1618} when the vWF protein is in the folded conformation. After initial unfolding, the stabilization from hydrogen bonding is lost and the proline residue undergoes isomerization to trans. Conversion to *trans*-Pro^{1645} notably delays A2 domain refolding and allows unfolded vWF to continue the process of blood vessel coagulation and repair [23]. The force-induced unfolding of vWF shows an

organized process involving mechanoscissions of covalent and noncovalent bonds, hydrophobic interactions, and subsequent isomerization.

1.2.3 Stress Mitigation by Tissue

Biological tissue has shown to undergo stress mitigation to avoid complete material failure through the use of noncovalent interactions. One specific example is the metal–ligand interactions in the outer coating of byssal threads in marine mussels [24, 26]. These byssal threads are secreted as bundles of 50–100 individual threads and are covered in a proteinaceous outer coating, called the cuticle, which is five times stronger than the internal threads themselves. Mussels use byssal threads to attach to rocks; the cuticle's toughness prevents the byssal threads from disconnecting following applied force. The primary cuticle protein is a modified tyrosine, which includes the molecule 3,4-dihydroxyphenylalanine (dopa). Included among the proteins are naturally existing metal ions, such as iron and calcium. Up to three dopa ligands can crosslink to the iron(III) ions (Fe^{3+}), resulting in an increased hardness (Figure 1.3). Granules are areas of high-concentration dopa-Fe^{3+} crosslinking within the cuticle. Lighter dopa-Fe crosslinking occurs in the matrix surrounding the granules. Following increased strain (>30%), the granules deform slightly, whereas the surrounding matrix crosslinks dissociate, forming microcracks. These microcracks allow the cuticle to absorb mechanical force without complete fracture. Following removal of strain, the granules instantly regain their original shape, while the microcrack crosslinks slowly self-heal over time.

1.2.4 Sensing by Ion Channel Opening

Mechanotransduction is important for signaling in sensory systems. Hair cells in the ear called stereocilia are mechanosensory biological structures that convert mechanical energy from sound waves into electrochemical signals that can be processed by the nervous system as hearing [19]. Stereocilia are linked together at their tips into bundles by proteins called tip links. These tip links are anchored into the cell membrane connecting an ion channel of one stereocilia to the tip of another [27]. Vibrational perturbations from sound deflect stereocilia tips cause opening and closing of ion channels (Figure 1.4). Opening and closing of the channels result in a change of ion flux leading to an electric potential that can stimulate the auditory nerve [28].

Another fascinating example of mechanotransduction in human senses is found in the mechanism of touch. Touch is essential for life as tactile input guides behavior. Discriminative touch allows uniquely human activities where finesse is needed. Delicate touch is allowed by the many sensory receptors imbued in the skin. A diversity of somatosensory neurons in the skin allows for a variety of sensations by taking advantage of varying mechanical thresholds in different proteins. For example, light touch is mediated by Aβ afferents that have a low mechanical threshold compared to the high mechanical threshold of nociceptors that mediate painful touch [29]. Moreover, an assortment of mechanoreceptors under the skin detects stretches,

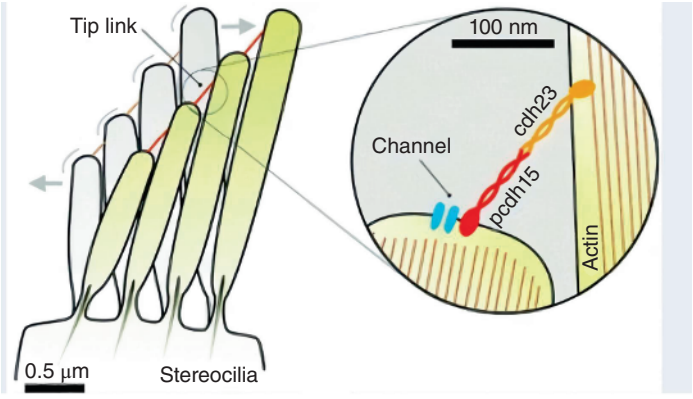

Figure 1.4 Illustration showing sensory cells called stereocilia located in the inner ear of mammals. The stereocilia deflect back and forth upon mechanical stimulation by sound waves. Source: Hoffmann et al. [27]/with permission of Royal Society of Chemistry.

vibrations, slip, and motion that enable us to determine an object's shape and texture. Little is known about the mechanisms for mechanotransduction in touch; however, the recent discovery of piezo proteins may help better understand how proteins are activated by membrane deformation. Piezo proteins are ion channels mechanically activated by touch, suction, and shear stress [30]. High concentrations of piezo proteins around receptors and neurons implicate their responsibility for encoding transduction channels in touch receptors.

As can be seen from these examples, mechanoresponsiveness in biological systems relies on mechanotransduction, which transforms mechanical energy into a biochemical signal that induces specific cellular responses, which frequently takes advantage of noncovalent interactions [19]. Also commonly found in living systems are kinetically trapped states that are structures locked far away from thermodynamic equilibrium in a high-energy conformation, such as folded proteins or prestressed cell membranes [31]. Organisms take advantage of these structures to enable sophisticated dynamic responses to force. Precisely mimicking biological structures and mechanisms is challenging and unnecessary because of the complexity. However, similar mechanoresponsive bonding domains utilizing the chemistry and structure characteristics learned from biomacromolecules can be employed, and living-like functionaries can be created through the design principles of synthetic materials.

1.3 Mechanistic View of Mechanochemistry

One of the most interesting aspects of mechanochemistry is that it yields products that are different from thermal- and photo-reaction pathways. This phenomenon has been observed in both inorganic and organic compounds. Here, we will use an extensively studied mechanochemical reaction, the pericyclic reaction, as an example

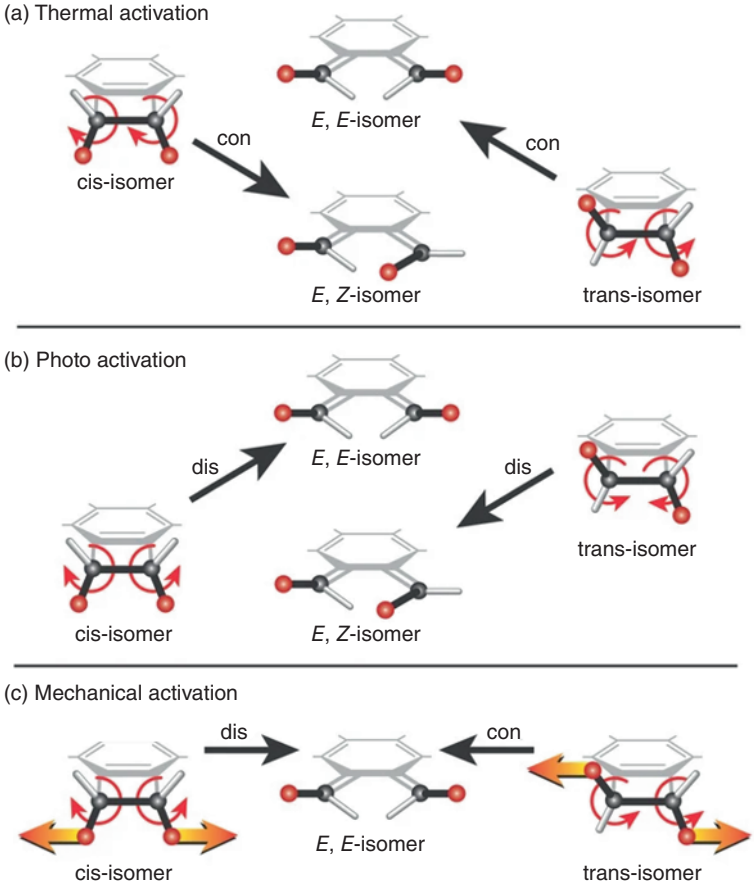

Figure 1.5 Ring opening of 1,2-disubstituted benzocyclobutenes (BCB) under different energy inputs. Source: Hickenboth et al. [32]/with permission of Springer Nature.

to discuss its mechanistic origin. Thermal activation of 1,2-disubstituted benzocyclobutene (BCB) induces conrotatory (con) ring openings, so that the cis and trans isomers give different ring-opening products (Figure 1.5a). When activated by light, disrotatory (dis) ring opening is favored instead of con for both cis and trans isomers (Figure 1.5b). This stereospecificity under thermal and photo-activations is described by the well-known Woodward–Hoffmann (WH) rules. However, when BCB is placed within long polymer chains, the mechanoproducts do not follow WH rules [32]. Mechanical forces induce a formal disrotatory ring opening in the cis isomer and a formal conrotatory ring opening in the trans isomer, yielding the same *E*,*E*-isomer (Figure 1.5c). The lack of selectivity was also observed for mechanoactivation of *gem*-dihalocyclopropanes [33–35]. If the force is viewed as pulling in opposite directions at the two molecular anchoring points, the reaction pathway favors bond breaking to increase the distance between the pulling points.

These stunning mechanochemical phenomena intrigued the study for the underlying mechanisms. Photoirradiation activates thermally forbidden pathways by promoting the reactants to electronically excited states. Force, however, does not directly alter the energy of the electrons. Thus, how does mechanochemical reaction overcome the WH rule? This is discussed in great detail in several studies via quantum chemical methods [36–39]. The results show that applied stresses do not alter the electronic structure. Instead, they lower the activation barrier for WH-forbidden pathways. Figure 1.6 shows the minimum energy pathways for mechanical ring opening of BCB under various forces from quantum chemical calculations [36]. For directional pulling of the cis isomer, beyond a critical force of 1.5 nN, the barrier for WH-forbidden disrotatory pathway drops below the conrotatory pathway, and disrotatory becomes the mechanically favored pathway. For the trans isomer, conrotatory is favored. Therefore, the two isomers yield the same ring-opening products as shown in Figure 1.5c. Since mechanical work alters the potential energy surface (PES), lowering the activation barrier without changing electronic structures, electronic considerations, such as WH rules, is not directly applicable.

The next question is how much force it takes to break a chemical bond. Mechanical strength of macroscopic materials can be characterized by a rupture force. This holds true for single chemical bonds only if they do not undergo any vibrations. The bonds will rupture when dissociation force exceeds the bond strength. However, bonds undergo thermal fluctuations. Combined with a pulling force, they led to a far more complex dependence on force conditions. Developed to describe the strength of cell adhesion, the well-known Bell's model provides a simple explanation for the effects of stress on bond rupture [40]. When a bond is pulled, the mechanical force deforms the PES, reducing the activation energy for bond rupture, which can be overcome by additional energy from thermal fluctuations. As a result, molecular bonds have no single rupture force, which is not so intuitive. Mathematically, Bell's model is described as

$$\tau = \tau_0 \exp[(E_0 - \gamma f)/kT]$$

where τ is the lifetime of a bond, which is the reciprocal of oscillation frequency, and τ_0 is the bond lifetime without load. The change of activation energy is expressed by $E_0 - \gamma f$, where E_0 is the bond energy at zero force, f is the applied force, and γ is a structural parameter that accounts for the distance to the transition state along the reaction coordinate. Thus, the activation barrier changes linearly with force, and the bond lifetime decreases exponentially with increasing force and temperature. Based on this equation, it was proposed that force impulse is the highest when $F = kT/\gamma$ at which force transduction is maximized [41]. A limitation in applying Bell's theory to computational calculations is the selection of the structural parameter γ. Since γ itself is force dependent, the model fails to account for the mechanically induced distortion of transition-state geometry, resulting in an overestimate of the bond rupture rate when there is considerable elongation of the scissile bond. Many extensions have been developed to improve Bell's theory. The extended models along with other quantum chemical treatments to understand the relations of geometries, energies,

and transition states in mechanochemistry are summarized in a review article by Stauch and Dreuw [42].

Experimental studies evolved parallelly with the theoretical predictions to measure the rupture force of a single bond. In late 1990s, the use of atomic force microscopy (AFM) made it possible to probe the mechanical responses of covalent and noncovalent bonds in a single macromolecule [43–48]. Force responses are probed on a nanoscale with forces on nano Newton (nN) to sub-nN levels. In a force-probe AFM experiment, the molecule is anchored between a surface and an AFM tip. It is then stretched at a constant force rate until rupture [48]. A force–extension curve for a single chemical bond is thus generated, which reveals conformational changes, supramolecular rearrangements, along with bond rupture steps. Bond rupture of the BCB, which is shown in Figure 1.6, is measured using single-molecule force microscopy [49]. It provides the first experimental evidence

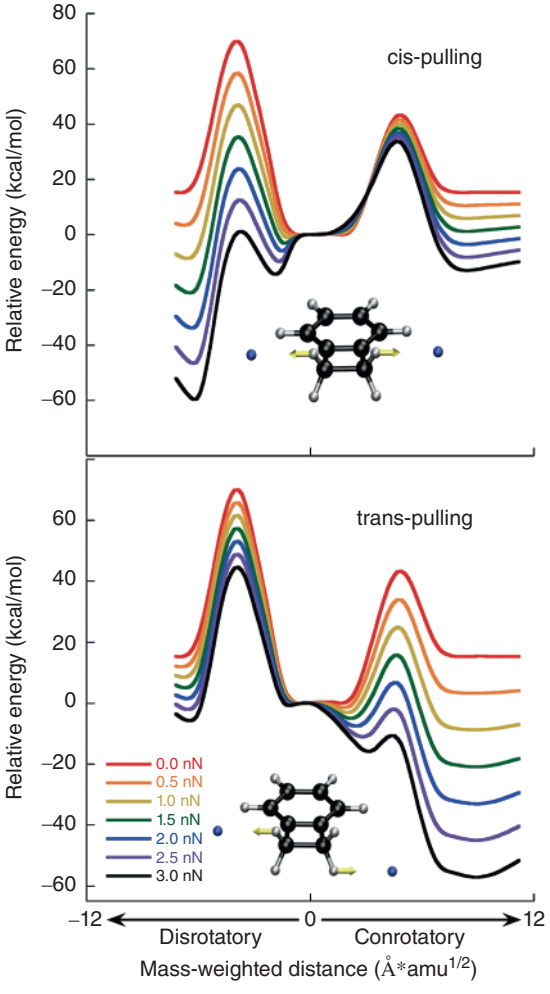

Figure 1.6 Minimum energy pathways for disrotatory and conrotatory ring opening of BCB under various force magnitudes calculated via steered molecular dynamics combined with *ab initio* steered molecular dynamics (AISMD). Source: Ong et al. [36]/with permission of American Chemical Society.

that the symmetry-forbidden conrotatory ring opening can be mechanically accelerated, requiring a 130 pN less force compared to disrotatory pathway at a ~0.1 second experimental timescale.

Force dependency of reaction rate can also be measured using single-molecule force spectroscopy. A constant force is applied, and the deformation is recorded as a function of time. This approach is called force-clamp AFM. The technique has been used to study the kinetics of thiol/disulfide exchange reactions within a protein [50]. The reaction is known to occur during protein unfolding in mechanically stressed proteins and is crucial in regulating protein function. The experiment utilized protein engineered with a precisely positioned disulfide bond. Disulfide reduction events can thus be correlated with a signature protein contour length, which can be identified in the extension experiment. As shown in Figure 1.7a, mechanical force first triggers the unfolding of the protein (unsequestered unfolding), exposing the disulfide bond. In the presence of a reducing agent, 1,4-DL-dithiothreitol (DTT), the disulfide reduction occurs. The rates of the biomolecular reduction were measured by fitting the extension-time curve signaturing the disulfide exchange under varying force magnitudes. The exchange rate showed an exponential increase with the applied force (Figure 1.7b). Fitting the experimental results using Bell-like model gives a γ value, the lengthening of the transition state, of 0.34 Å. An energy landscape is plotted showing an 8.2 kJ/mol reduction of activation energy when a 400 pN force is applied (Figure 1.7c). The reversibility of disulfide exchange was recorded by force-clamp AFM [51]. Mechanical force enabled the thermodynamically unfavorable S_N2 substitution of a disulfide with weak nucleophilic thiols. Upon removal of load, the bonding returned to the original disulfide of lower energy. Reversibility is critical in mechanical-responsive materials so that perturbations can be repeated in a highly dynamic manner.

Going back to Bell's model, as a bond undergoes constant thermal fluctuations, how fast the force is applied relative to the thermal fluctuation affects the breaking force. Therefore, bond-breaking force is dependent on the force-loading rate (df/dt). This dependency can be characterized into three regimes, the spontaneous, force-assisted, and activationless regimes, as shown in Figure 1.8 [52, 53]. When the loading rate is low relative to bond thermal dissociation rate, bonds break spontaneously due to thermal fluctuations. This is called a spontaneous regime. In this region, the breaking force is low and independent of the force rate. Bonds with rapid thermal oscillations and short bond lifetime, such as host–guest interactions, fall within this regime [54]. As force rate increases, it becomes sufficiently fast that the bond is stretched to some extent before breaking. This is called the force-assisted regime, and the breaking force increases rapidly with force rate. This has been observed for avidin–biotin complex [55], H-bonded carboxylic acid groups [56], and gold–octanedithiol–gold links [57]. In the activationless regime under high-loading rate, the energy barrier to breaking is reduced to zero as the bond is maximally stretched, and bond breaks solely by the applied force. In this region, the breaking force reaches the highest and becomes constant again. While single-molecule experiments allow us to validate the theoretical predictions, caution must be used when comparing the rupture force values, which are highly dependent on experimental

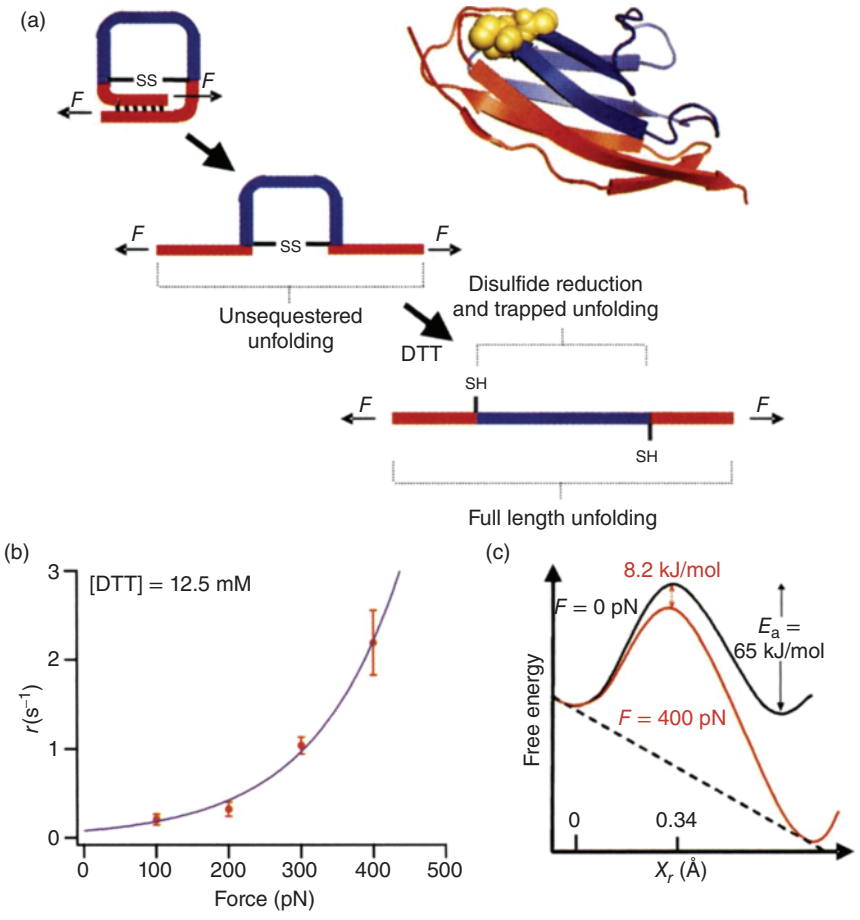

Figure 1.7 (a) Unfolding and disulfide (SS) reduction for an engineered protein with a precisely positioned disulfide bond. (b) Rate of reduction of the disulfide bond as a function of applied force measured by force-clamp AFM. Concentration of the reducing agent, DTT, is kept constant at 12.5 mM. (c) Calculated energy landscape with and without forces. A 400 pN force reduces the activation energy of disulfide reduction by 8.2 kJ/mol. Source: Wiita et al. [50]/with permission of National Academy of Sciences.

conditions. A comprehensive review by Ribas-Arino and Marx summarized the single-molecule spectroscopy and the theoretical treatments in great detail [58].

In the context of bulk polymers, sensitivity of the mechanoresponsive bonds becomes dependent on force transduction and heterogeneities of force distribution. For a single chain, the weaker bonds break first followed by the stronger bonds. The rupture forces for common covalent bonds are within a few nN (Figure 1.9) [59]. For noncovalent interactions, the rupture forces are in a much lower range, around 10–100 pN [58]. When mechanocleavable bonds are placed within a polymer strand, however, the force transduction can be far more complicated. An often-asked question is which bond is most likely to rupture within a polymeric material under mechanical deformation. This is determined by both the bond strength and the

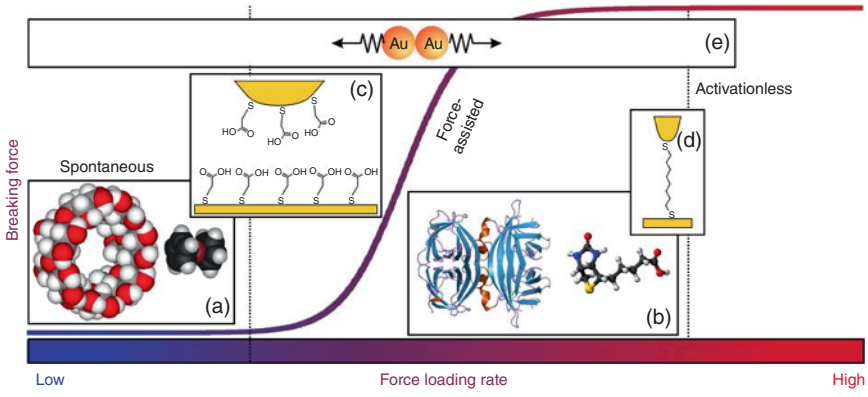

Figure 1.8 Dependence of bond-breaking force on force rate. (a) Host-guest complex representative of spontaneous breaking. (b) Bindings between biomolecules such as avidin and biotin representative of force-assisted breaking. (c) Hydrogen bonding between carboxylic acids falls within the transition regime from spontaneous to force-assisted breaking. (d) Gold-octanedithiol-gold interaction falls within the transition regime from force-assisted to activationless breaking. (e) breaking of the bond between two gold atoms at room temperature spans across the entire spectrum. Source: Pobelov et al. [52]/with permission of Springer Nature.

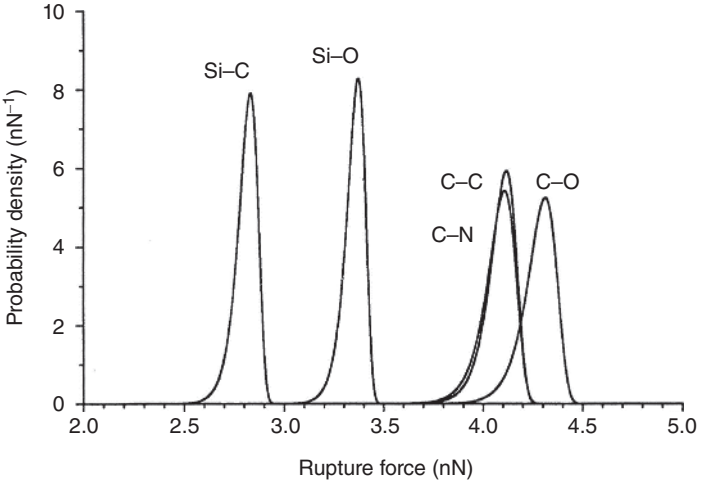

Figure 1.9 Bond rupture probability densities (nN^{-1}) as a function of force F (nN) calculated by density functional theory. Force-loading rate is 10 nN/s. Source: Beyer [59]/with permission of American Institute of Physics.

force distribution. The former can be predicted or measured, the latter is anisotropic within a polymeric material. One study incorporated coumarin dimer (CD) into specific locations of well-defined polymers as a means to determine the role of mechanophore spatial distribution on the efficiency of mechanoactivation [60]. The experiment was carried out in solution under ultrasonication. When CD was incorporated near the center of a chain, selective breaking of the CD dimmer

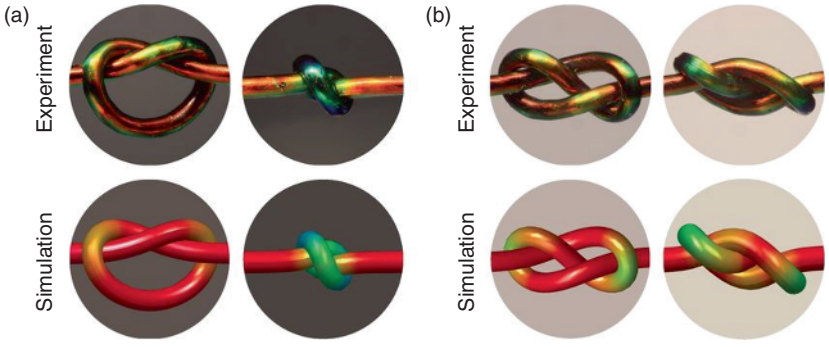

Figure 1.10 Color-changing mechanoresponsive fibers confirm the stress patterns predicted by continuum simulations for the trefoil knot (a) and the figure-of-eight knot (b) during the tightening process. The color is coded in the CIE 1931 XYZ color space. Approximately red end of the spectrum corresponds to low strain and the blue end corresponds to high strain. Source: Reproduced with permission from Patil et al. [63]/American Association for the Advancement of Science — AAAS.

occurred. However, when the CD was located away from the chain center, random cleavages of backbone bonds were dominant. In the solid state, force transduction is further complicated by entanglements, knots, and other defects. Early studies suggested that the highest stress is formed at the entrance position to the knot [61]. However, the chains considered in this simulation are relatively short; thus, it is possible that being close to the chain end also contributes to the high stress at the immediate vicinity of the knot. When polyethylene of 40 carbon atoms is simulated for end-to-end stretching, the stress is concentrated at the torsions around the curved part of the knot [62]. A mechanistic study of tying ropes into different topologies [63] may shed some light on this disagreement. Figure 1.10a, b shows a color-changing photonic fiber with two different knots. The fiber is coated with a periodic cladding. When the knot is tightened, thickness of the cladding changes upon elongation or bending, leading to color variations. Note this is a structural color and does not involve any mechanochemistry. Moving from the red to the blue end of the color spectrum, both strain and stress increase, and the stress is localized at the curved parts of the tightened knot. The stimulation results show a similar stress distribution pattern. Interestingly, the study showed that the stress localization within the knot can be more substantial for certain knots than others under the same pulling force. If we draw an analogy of entangled polymer chains with knotted ropes, one can clearly see the extent of anisotropy in stress distribution. Additionally, cumulative forces of numerous intermolecular interactions with certain configurations can shield a weak bond from mechanical activation. Crystalline domains, covalent crosslinks, physical crosslinks, and topological defects, such as loops, can further contribute to the heterogeneities. The effects of side groups, backbone rigidity, backbone creep, and relaxation cannot be neglected either. Furthermore, an interesting behavior is that the cleavable bonds do not have to directly align with the pulling axis. This is further discussed in Section 1.4 of this

chapter. Therefore, the complex and rich behaviors of polymer mechanochemistry are an area to be further explored.

1.4 Polymer Covalent Mechanochemistry

In this section of the chapter, we will consider mechanical activation of numerous mechanophores based on covalent bonds within polymeric materials. Such labile covalent bonds include C—C, C-heteroatom (e.g. C—O, C—S, C—N, C—Cl, and C—Br), and heteroatom–heteroatom (e.g. O—O, S—S, and Se—Se) bonds. The covalent mechanophores described in this section are classified as pyrans, retro-cycloadditions, ladderenes (LDEs), stable radical systems, and other types. The mechanochemical rupture can generally occur via pericyclic (e.g. electrocyclic ring opening of pyrans and retro-cycloadditions), homolytic (e.g. radical formations), or heterolytic (e.g. benzoxazole [Bz's] ester bond cleavage) reactions. The occurrences of mechanochemistry are often associated with distinctive changes in materials' properties which can be utilized to perform certain functions. For example, color change and fluorescent emissions are involved in mechanoactivation of pyran-based compounds. Such mechanophores are termed mechanochromophores and mechanofluorophores, and they enabled the detection and mapping of stresses in polymer materials [64–67]. Mechanoradicals are generated via homolytic cleavage of covalent bonds under force and have been employed in polymerizations to enable self-healing properties [68]. Ultrasonication-induced selective cleavage of disulfide-centered polymers gave thiol-terminated polymer chains, which could then undergo thia-Michael addition to Diels–Alder adducts of furan-functionalized drugs and acetylenedicarboxylates, followed by a retro-Diels–Alder reaction in which the liberation of a small molecular drug occurred [69]. Likewise, another study reported on a release of an alkaloid-type anticancer drug by an intramolecular cyclization of mechanochemically generated thiol-terminated polymers [70].

Constrained-geometry-simulating external force (CoGEF) [59] that is based on density functional theory (DFT) has been carried out to computationally determine the threshold forces required to activate covalent mechanophores. In this CoGEF method, the system begins with an unstrained state of the mechanophore. Two anchoring points from the opposite sides of the mechanophore are then selected, the distance between these two points is increased in small steps, and the geometry with the minimum energy is identified for each elongation step. A plot of relative energy versus equilibrium displacement is subsequently constructed, and the threshold force is extracted from the slope of the plot just before the bond cleavage occurs. The threshold activation forces for numerous mechanophores have been assessed via CoGEF calculations, and the predictive power of this method for polymer mechanochemistry has been demonstrated [71]. For a range of mechanophores, the CoGEF predictions are in good agreement with the experimental values obtained from the single-molecule force spectroscopy measurements. In this section, we will focus on discussing the chemistries involved and the tunability of the bond dynamics.

1.4.1 Pyran-Based Mechanochromophores

Spiropyran (SP) is a well-known photochromic molecule. Under UV radiation, the colorless and nonfluorescent SP undergoes 6π electrocyclic ring opening to form merocyanine (MC) species (Scheme 1.1). The increase in conjugation in MC shifts the absorption to longer wavelengths, giving rise to visible color and fluorescence [72]. Ring opening of SP can also be mechanically activated when incorporated into polymer backbones by tethering its two ends. Under uniaxial stress, the conversion of SP to MC resulted in a color change of the polymer from yellow to purple and to red once failed [72]. SP-functionalized polymeric materials have also shown mechanochromism induced by grinding, ultrasonication [73], and shear stress [74]. Even though SP incorporated polymers are typically colorless or yellow, their MC forms can show different colors, such as blue, purple, or red, under different strains. As shown in Figure 1.11, the polymer turned blue when stretched. Upon release, its color changed to purple via the isomerization of the methine bridge that links the two cyclic components [75]. The colorless form is restored after radiation with visible light.

It is crucial that the tensile stress is applied across the spiro-junction to pull apart the indoline and benzopyran moieties to exclusively cleave the C_{spiro}—O bond. This can be achieved by tethering the polymer chains to the opposing sides of the spiro-junction, such as positions 7 or 8 of the benzopyran and 5′ or 6′ of the indoline [72]. Functionalizing SP at other positions, such as 1′and 5′ of the indoline component, prevents the mechanical force transduction across the reactive

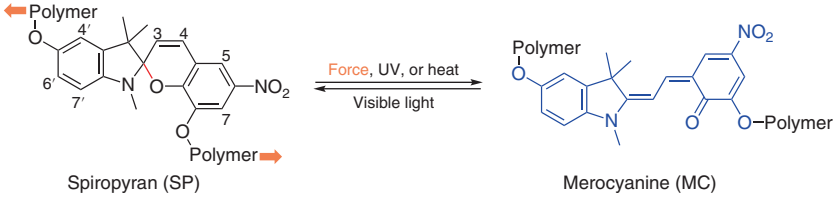

Scheme 1.1 Electrocyclic ring opening of spiropyran to form merocyanine.

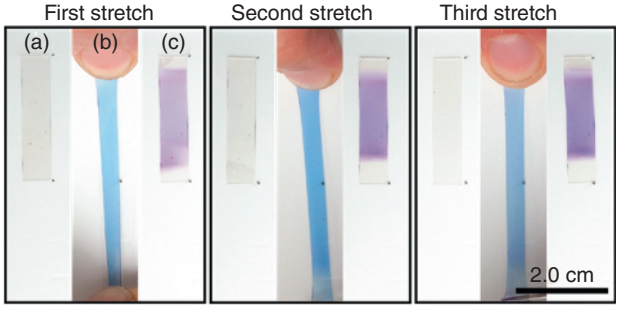

Figure 1.11 Original spiropyran sample is colorless (a) and turns blue when stretched (b). Once the sample is relaxed, it turns purple (c). Source: Reproduced with permission from Gossweiler et al. [75]/American Chemical Society.

C_{spiro}—O bond, although SP to MC transformation can still take place by heating or UV radiation [76]. Regiochemical effects on mechanical activation have been quantified by using two SP regioisomers via single-molecule force spectroscopy measurements [77]. In one isomer the polymer chains were tethered to positions 5′ and 8, while in the second isomer the polymer chains were attached to positions 8 and indole's N atom, and the threshold forces for activation were determined to be 260 and 240 pN, respectively. The rate of mechanochromism is governed by several factors that include the nature of the materials (e.g. elastomeric polymers have demonstrated faster decay of the color change than those of glassy ones) [72], local environment (e.g. temperature and plasticizers) [78], and substituents on the SP (i.e. the higher the electron density on the aromatic ring of benzopyran, the faster the ring closure) [79].

Spirothiopyran (STP), an SP analog, displays both mechanochromism and stress-induced addition reactions rendering it a versatile mechanophore. Ring opening of the thiopyran ring forms the corresponding thiomerocyanine (TMC) in its thiophenolate form (Scheme 1.2), which can take part in thiol-ene click reactions in the presence of olefinic double bonds. Ultrasonication-activated polyester-functionalized STP showed yellow to green color change because of the formation of the TMC form; however, the green color quickly faded in the presence of *N*-methylmaleimide due to the thiol-ene click reaction [80]. When *N*-methylmaleimide is replaced with the bifunctional 1,6-bismaleimidehexnae crosslinker, mechanical-induced crosslinking of the linear polymers was achieved, giving insoluble networks.

Mechanochromism can be affected by both electronic and steric effects. This is shown for naphthopyran (NP) in Scheme 1.3. The activated merocyanines not only exhibit different colors but also their threshold forces vary depending on the nature of the substituents. NP species (Scheme 1.3a) forms a yellow MC, whereas NP modified with electron-donating pyrrolidine (Scheme 1.3b) gives a purple MC [81]. CoGEF calculations indicate that electron-donating and bulky pyrrolidine decreases the activation force for mechanical scission [71]. Once the mechanical force is eliminated, heat-induced ring closure results in the reformation of NP and NP-Pyr.

As is true for SP and NP, oxazine (OX)-derived mechanophores also demonstrate regioisomer-dependent mechanochromism [82]. As shown in Scheme 1.4, the bulk

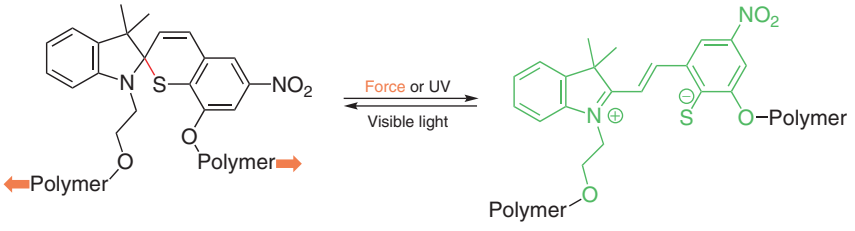

Scheme 1.2 Electrocyclic ring opening of spirothiopyran to form thiomerocyanine.

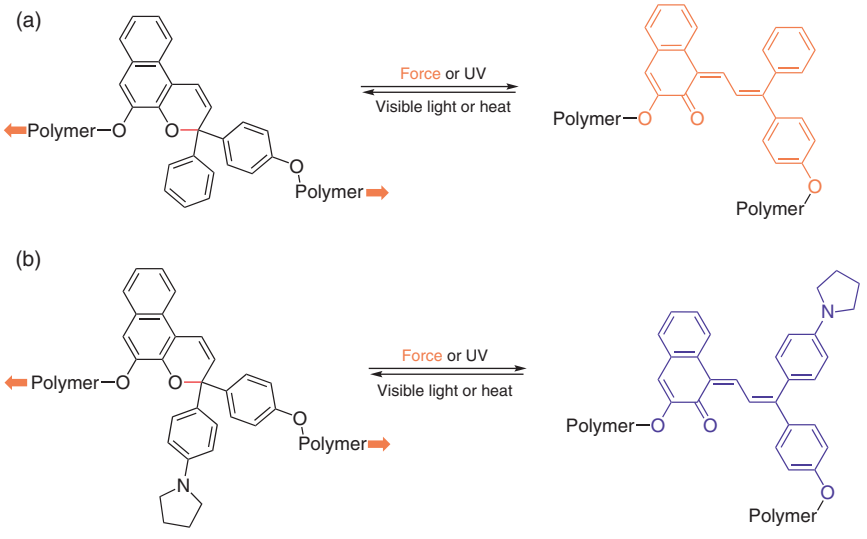

Scheme 1.3 Electrocyclic ring opening of (a) naphthopyrans (NP) and (b) pyrrolidine-appended naphthopyrans (NP-Pyr).

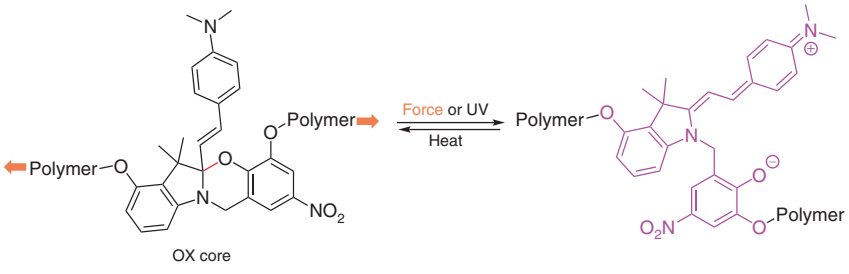

Scheme 1.4 Electrocyclic ring opening of oxazine to give zwitterionic indolium species.

polymer-embedded OX core undergoes mechanical stress-induced pericyclic ring opening to generate a colored, zwitterionic indolium isomer, which reverts to the ring-closed form upon removal of the tensile stress within less than a second. This markedly faster mechanoresponsiveness of OX without any phase lag or fatigue compared to SP or NP is striking. It should be noted that the ring opening of both SP and NP is followed by a double-bond isomerization process to form the corresponding *trans*-MCs, but such an isomerization does not take place with OX, which might explain OX's faster mechanoresponse. In comparison to SP or NP, OX mechanophore may hold better promise as a molecular force probe since OX has a shorter cleavage displacement (e.g. SP and NP frameworks need to be stretched about thrice as much as OX for the bond rupture) as well as its less complicated ring-opening process without the double-bond isomerization.

The above-mentioned mechanophores all contain one pyran ring and give the same mechano- and photo-product. Mechanochromic bis(naphthopyran) (BNP) featuring doubly closed pyran ring (BNP_{C-C}) configuration exhibits a different

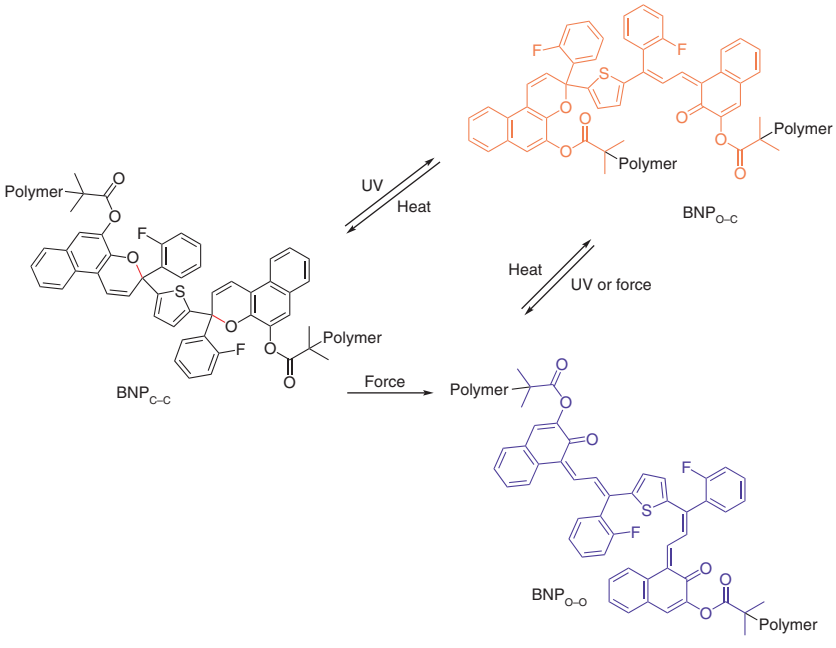

Scheme 1.5 Electrocyclic ring opening of bis(naphthopyran). UV irradiation leads to stepwise ring opening via BNP_{O-C}, while mechanical force directly transforms BNP_{C-C} to BNP_{O-O}.

mechanochemical pathway [83]. As shown in Scheme 1.5, under continuous UV irradiation, BNP_{C-C} undergoes ring opening of one of the pyran rings to first form an open–closed BNP_{O-C} MC species, followed by a fully open MC form (BNP_{O-O}). In contrast to this sequential photochemical ring-opening process, under mechanical activation, an equilibrium of BNP_{C-C}, BNP_{O-C}, and BNP_{O-O} is reached but through a different mechanism. BNP_{O-O} is formed directly from BNP_{C-C} by mechanical activation; therefore, its concentration is force dependent. BNP_{O-C} is produced predominately from the thermal electrocyclization of BNP_{O-O}. Meanwhile, BNP_{O-C} can be mechanically activated to generate BNP_{O-O} again. Therefore, the distribution of BNP_{O-C} and BNP_{O-O} varies with the magnitude of force. Since the two MC products have distinctly different absorptions in the visible range, BNP exhibits gradient multicolor mechanochromism, which can be used as a stress sensor. Systematic studies of these compounds have been conducted to illustrate the substituent effects [43, 71], stereochemistry, and regioselectivity [71]. Computation and experimental studies allow us to understand mechanisms of mechanochemical reactions, as discussed in Section 1.3.

1.4.2 Retro-Cycloadditions

In a cycloaddition reaction, two π reactants react to form a cyclic adduct that contains two new σ bonds. The adducts are susceptible for reverse reactions (i.e.

retro-cycloadditions) under sufficient mechanical force. Here, we will summarize the use of retro-cycloadditions in designing polymeric materials for sensing, release of small molecules, gated ring opening, and degradable materials.

Anthracene-derived Diels–Alder adducts have been widely used as mechanofluorophores because of their high fluorescent quantum yields. Anthracene dimers [84], anthracene–maleimide adducts [85–88], as well as π-extended anthracene–maleimide adducts [89] incorporated into polymers can be mechanically activated. The liberation of fluorescent anthracene derivatives takes place via stress-induced retro Diels–Alder of the anthracene adducts, which in turn leads to the scission of the polymer chains. Using this concept, anthracene–maleimide adducts have been employed as damage sensors at heterointerfaces [90, 91]. An anthracene–maleimide adduct-embedded polymer chain was grafted onto the surface of silica nanoparticles. Here, anthracene species was liberated via ultrasound. This showed the selective rupture or activation of mechanophores under mechanochemical stress at a heterointerface. The mechanochemical activation of π-extended anthracene–maleimide adducts (Scheme 1.6a) is particularly interesting because they give a fluorescence quantum yield of 0.72, which is about 2 orders of magnitude higher than those reported for merocyanines derived from spiropyrans [89]. Besides, the fluorescence is stable in the presence of excess oxygen and the system is not susceptible to thermal reversibility. The appropriate functionalization of this mechanofluorochromophore (via the substituents in anthracene) gives the opportunity to tune excitation and emission wavelengths while maintaining mechanochemical properties of the system. This highly sensitive π-extended anthracene–maleimide adduct was used as a crosslinker in a poly(*N*-isopropylacrylamide) hydrogel network to detect and accurately localize the covalent bond scission induced by a needle-puncturing (hand) [92]. Anthracene–maleimide adducts have been employed as damage sensors in polymers using them at heterointerfaces [90, 91]. For example, an anthracene–maleimide adduct-embedded polymer chain has been linked to a surface of silica nanoparticles, and ultrasound activation of the mechanophore has led to the liberation of the anthracene species thereby ensuring the rupture of the polymer chain.

Mechanochemical activation of the mechanophore-centered polymer chains not only yields optical responses but also can display chemical responses by the release of small molecular cargos, such as furans [93, 94], coumarin [95], and phenyltriazolinedione [75]. A difunctional crosslinker comprising mechanophore oxanorbornadiene, which is a Diels–Alder adduct of furan and acetylenedicarboxylate, was incorporated into a polymethyl acrylate (PMA) matrix in which compression-induced retro-[4 + 2] Diels–Alder reaction liberated the benzyl furfuryl ether small molecules (Scheme 1.6b) [93]. In this example, the cleaved covalent bonds were not an integral part of the polymer main chain, which is quite counterintuitive. The activation occurred by bond bending instead of stretching. Hence the overall polymer architecture is retained intact, while indeed reinforcing the bonds in the polymer backbone. Force-accelerated dissociation of unloaded bonds also occurred for phosphotriesters [96]. In another study,

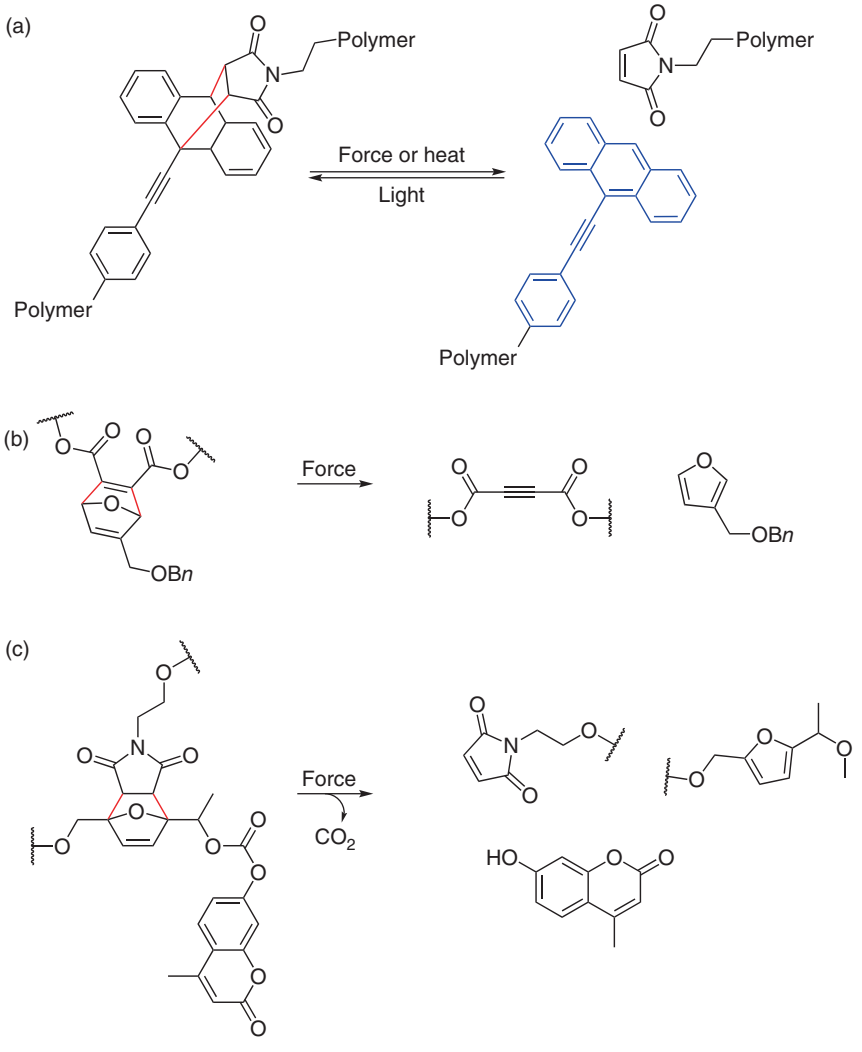

Scheme 1.6 Retro-cycloadditions under force. (a) π-extended anthracene–maleimide adduct. (b) Release of a furan derivative from oxanorbornadiene. (c) Liberation of a coumarin derivative from a furan-maleimide adduct.

a mechanophore, based on a furan-maleimide Diels–Alder adduct integrated into a PMA matrix, underwent a retro-Diels–Alder reaction under ultrasound to first form a polymer-chain-terminated unstable furfuryl carbonate intermediate, which underwent decarboxylation in polar protic solvents at room temperature, eventually liberating a covalently bound cargo molecule hydroxycoumarin, as shown in Scheme 1.6c [95]. Fluorescence spectroscopy can be used here to measure the mechanical activity since the hydroxycoumarin is fluorescent active. As the hydroxycoumarin is disconnected from the polymer chain, it can now diffuse freely

into the solution. The systems that enable release of molecular cargos should find applications in areas such as self-healing, depolymerization, and drug delivery [12].

A dual mechanophore – 5,5-dichlorotricyclo(7.2.0.0)undecane (DCTCU) has been employed to demonstrate a mechanochemically gated reaction, where one mechanophore (i.e. cyclobutane) served as a molecular gate to initially prevent the transmission of mechanical force to a second mechanophore, *cis-gem*-dichlorocyclopropane (*cis-g*DCC) [97]. Once the gate was mechanically removed, *cis-g*DCC could experience the force, which in turn led to a cascade of mechanochemical reactions. Thus, the two different mechanophores were designed to be activated in succession under sonication. It has been determined that a higher force is required for a DCTCU polymer (where *cis-g*DCC is gated) than that of a free *cis-g*DCC polymer for the mechanical isomerization of *cis-g*DCC to dichloroalkene to occur at an equal rate. The additional force required to first dissociate the cyclobutane gate before the activation of *cis-g*DCC agrees with the higher force necessary for DCTCU polymer. In a separate study, ultrasonication-induced mechanochemical activation of a thermally and photochemically stable cyclopentadiene-maleimide Diels–Alder adduct embedded polymer has been reported, where the adduct underwent retro-[4 + 2] cycloaddition to furnish dithienylethene photoswitch that could isomerize between colorless (ring-open) and colored (ring-closed) forms with UV and visible light, respectively [98]. The mechanophore (adduct) lacked a 6π electronic arrangement for cyclization, rendering it photochemically latent. Therefore, we can realize that mechanochemistry followed by photochemistry here offers the only way to achieve this transformation from the adduct to the ring-closed form of dithienylethene. Note that the example shown in Scheme 1.6c was yet another scenario where mechanochemical gating has been exploited. According to these examples we discussed, mechanochemical gating shows promise to be applied in various areas, such as stress sensing, release of small molecules, catalysis, and tracing of the mechanical history of bulk polymers [97, 98].

Traditional degradable polymers usually contain reversible dissociable bonds on the backbone of the polymer. However, these cleavable bonds can be susceptible to external stimuli (e.g. light and pH) under ambient conditions, making the polymer material less stable. Therefore, polymers that demonstrate both durability and degradability can be difficult to implement. To tackle this conundrum, degradability can be "locked" during the use of a polymer, while it can be "unlocked" when degradation is required. To achieve this goal, a cyclobutane mechanophore-fused lactone polymer (poly(CBL)) has been employed [99]. Here, cyclobutane kept the polymer backbone intact (i.e. cyclobutane served as a "lock" or "gate") under lactone labile conditions (i.e. strongly basic), while the lactone function could be fully restored from the hydrolyzed product and hence the molecular weight of the polymer was not affected. To degrade the material, poly(CBL) could be mechanochemically "unlocked" that resulted in a copolymer of CBL and a linear polyester, which could be degraded under alkaline conditions. A similar study was simultaneously reported on a degradable polymer functionalized with a cyclobutane-fused cyclic acetal [100]. These two examples demonstrate a promising application of cyclobutane-based mechanophores in mechanoresponsive degradable polymers.

1.4.3 Ladderenes

In response to mechanical forces, cyclic rings, such as cyclopropane [97] and cyclobutenes [36], undergo electrocyclic ring opening and structural rearrangements. The mechanical activation of these mechanophores results in the formation of double bonds in the backbone, which results in significant increases in their mechanical properties or conductivities. For example, 2,3-dihaloalkenes are generated from *g*DCC. These double bonds can potentially take part in force-induced crosslinking that can reinforce the materials [101]. Also featuring formation of double bonds via mechanoactivated bond rupture, another class of well-studied covalent mechanophores is polyladderene (PLDE), which demonstrates an entirely distinct type of functionality than the above monocyclic species. A molecular zipper, PLDE, is synthesized from ring-opening metathesis polymerization (ROMP) of the LDE that consists of multiple fused cyclobutene rings (see Scheme 1.7a) and can be mechanically unzipped [102]. Formation of PLDE is driven by relief of the ring strain in cyclobutene. The ROMP provided a π-bond containing polymer backbone where the PLDE mechanophore was efficiently incorporated in the center of the polymer. Under sonication, the formation of highly conjugated polyacetylene (PA) block copolymers with a uniform *trans*-olefin configuration from nonconjugated soluble PLDE has been reported (Scheme 1.7b). This particular transformation could not be achieved with heat or light. PA-centered and PLDE termini ABA-type triblock copolymers were expected to form via the mechanical unzipping taking place from the middle of the polymer chain, where the mechanophore was embedded. The colorless PLDE solution initially turned blue after 20 second of sonication, and after sonicating for two hours, it became dark blue with simultaneous formation of black precipitate. A set of PLDEs with varying molecular weights was employed to prove their mechanochemical activation to yield PAs. For example, the formation of PAs took place more slowly as the size of the PLDE decreased though the absorption profiles were the same regardless of the polymer size. The mechanochemical nature of this process was hence validated because the thermal activation did not depend on the size of the polymer. The generation of highly conjugated (i.e. more than 100 conjugated C=C bonds) *trans*-PA was inferred according to Raman and UV–Vis absorption spectroscopy. The resulting PA polymers underwent self-assembly presumably via π–π stacking interactions to generate semiconducting nanowires with a measured conductivity of 2.6×10^{-7} S/cm. Ultrasonication-induced formation of semiconducting fluoropolyacetylene from fluoropolyladderene polymechanophore has also been reported [103].

This family of mechanophores holds high potential due to the ability of the monomer (i.e. LDE) to undergo direct polymerization, easy mechanochemical activation of PLDE, and substantial alteration of polymer properties upon mechanoactivation. Nevertheless, difficulties in synthesis (i.e. synthesis of chloroladderene monomer LDE was hard with a poor overall yield, and the yields were limited to milligram amounts) [102, 104] and derivatization are some of the drawbacks of this class. In addition, since ROMP is followed by an HCl elimination to yield the PLDE it could result in the shortening of some polymer backbones,

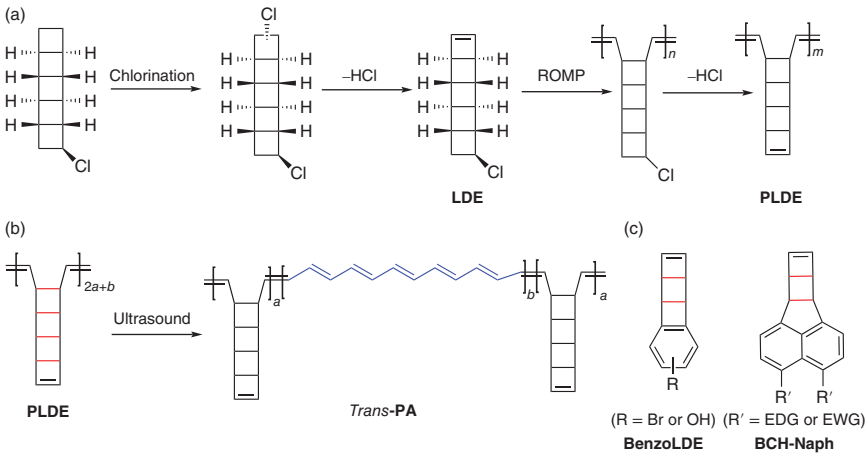

Scheme 1.7 (a) Synthetic scheme for the formation of polyladderene via ROMP (third step) followed by elimination of HCl (last step). (b) Formation of conjugated polyacetylene from polyladderene by mechanical stress. (c) Chemical structures of benzoladderene (left) and bicyclohexene-peri-naphthalene (right).

which in turn results in a broad molecular weight distribution [102]. Therefore, benzoladderene (benzoLDE, Scheme 1.7c, left) was introduced to address the above limitations [105]. Synthesis of the monomer as well as the poly(benzoLDE) was easier (i.e. higher overall yields for benzoLDEs and gram quantities could be synthesized) and could achieve better functionalization with benzoLDE compared to LDE. Furthermore, a more controlled polymerization (i.e. narrower dispersity) was observed with p(benzoLDE) because the ROMP process was not followed by an elimination step for p(benzoLDE) as opposed to PLDE.

An even superior ladder-type mechanophore called bicyclohexene-*peri*-naphthalenes (BCH-Naph, see Scheme 1.7c, right) that can also be effectively polymerized via ROMP to yield polymechanophores (p(BCH-Naph)) with extremely high molecular weights with low dispersity has been introduced [106]. Like PLDE and p(benzoLDE) mechanochromophores, p(BCH-Naph) also transforms into conjugated polymers upon exposure to mechanical stress. The ability to synthesize in multigram scale, broad functionality with both electron-donating and electron-withdrawing groups, enhanced stability, efficient polymerization of BCH-Naph as well as versatile mechanoactivation of p(BCH-Naph) via ultrasonication, stirring, and grinding renders p(BCH-Naph) an excellent polymechanophore reported in the literature.

1.4.4 Stable Radical Systems

A covalent bond can undergo force-activated cleavage to generate two free radicals. These radicals are usually short-lived and are readily quenched. However, when the radicals are stabilized, they can serve as mechanochromophores by the formation of colored radicals. The dramatic color changes accompanied as the radicals are formed

provide a way to qualitatively visualize the mechanical stress, while the use of electron paramagnetic resonance (EPR) measurements enables quantitative detection of radical species both in solution and bulk materials. The use of nitrone spin traps also provides a means to quantify the mechanically generated radicals with a colorimetric response [107]. Therefore, they can serve as probes for detecting and evaluating the stress experienced by the polymer materials. Stable radical systems are also utilized in self-healing materials. Mechanical damage causes scissions of sacrificial covalent bonds in the network, resulting in the generation of a large number of free radicals. By controlling their reactivity, self-healing can be achieved by either free radical combination [108–111] or initiation of polymerization when vinyl monomers are present [68].

The radical-based mechanophores can be broadly classified as carbon- and heteroatom-centered radical forming systems. For the formation of radicals from radical-type mechanophores described in this section, it is critical that the weak, central cleavable bond, such as C—C bond, possesses a lower bond-dissociation energy (BDE) than covalent bonds in the polymer backbone to enable exclusive cleavage. Typical BDE of a C—C bond is c. 350 kJ/mol. The reduction of the BDE is achieved by introducing bulk side groups to prestretch the target C—C bond and the resonance stabilization of the generated radicals via the neighboring groups, such as aromatic rings, heteroatoms, and carbonyl groups. Stability of the radicals can be further enhanced by incorporating them into polymer chains with high glass transition temperatures (T_g) to minimize recombination of the radicals. It leads to superior mechanochromism compared to just the mechanophores themselves. Scheme 1.8 lists the radical-based mechanochromophores that have been studied.

Diarylbibenzofuranone (DABBF) is a homodimer of arylbenzofuranone linked by a central head-to-head C—C bond (Scheme 1.8a). The bond length and BDE of the central C—C bond are 1.586 Å and 95.4 kJ/mol, respectively, suggesting it is much weaker than that of a typical C—C bond [112]. When incorporated into polyurethane as a mechanochromophore, it formed blue-colored arylbenzofuranone radicals under tensile stress via homolysis of the central C—C dynamic covalent bond, as shown in Figure 1.12 [113]. A similar mechanoactivated C–C scission was observed for tetraarylsuccinonitrile (TASN) [114] and diarylbibenzothiophenonyl (DABBT) [115]. Their structures are shown in Scheme 1.8b,c. The color of the radicals is pink for TASN and green for DABBT. The central C—C bond in TASN is somewhat longer (i.e. 1.608 Å); nonetheless, its BDE is 110 kJ/mol, which is higher than that of DABBF [112]. This higher BDE is consistent with a higher threshold force of 4.5 nN predicted by CoGEF [71]. The central C–C of DABBT has a BDE of 96 kJ/mol and this value can be modified by the substituents on the phenyl ring, for example, for the para-bromo-functionalized DABBT, the BDE is dropped to 86 kJ/mol [116]. The stable free radicals formed can be quenched by adding a good solvent that helps improve the molecular mobility or heating above the T_g of the polymer.

The poor thermal stability of the radical-based mechanochromophores described above limits their applications. Particularly, these radical-type mechanophores cannot be concurrently employed with free radical polymerization methods because the formed radical species can act as radical scavengers. For this reason,

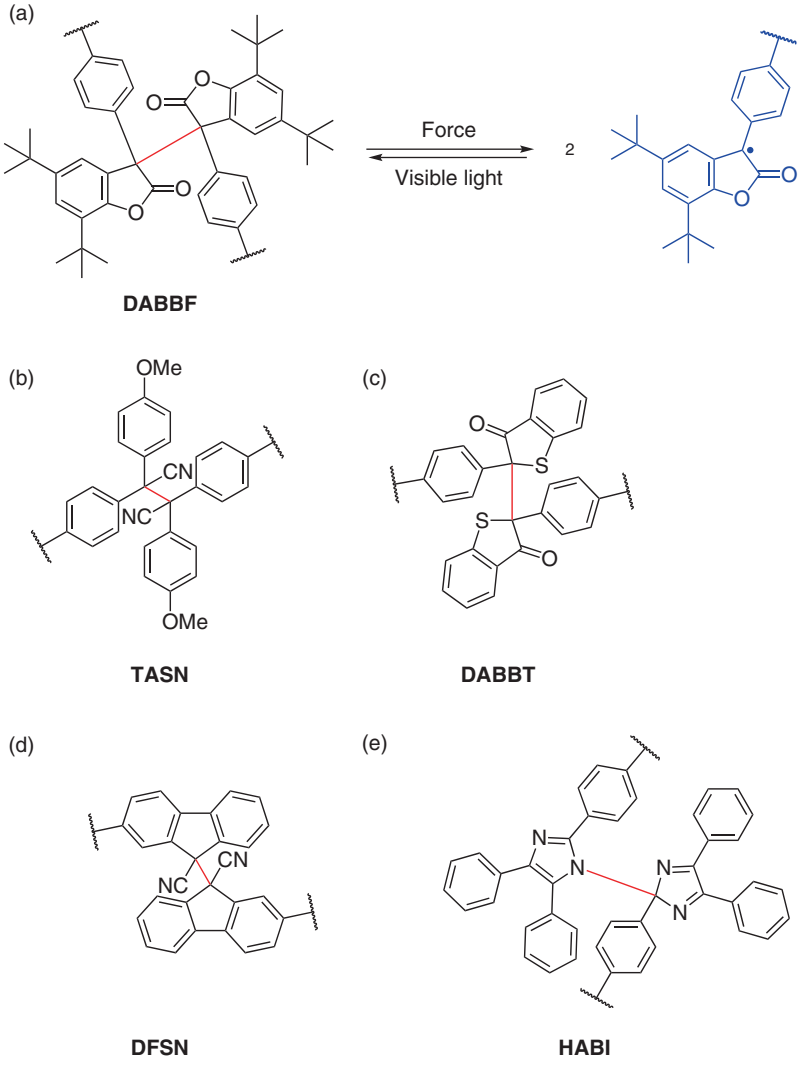

Scheme 1.8 Radical-based mechanochromophores. (a) Mechanical activation of DABBF gives colored radicals. Chemical structures of (b) TASN, (c) DABBT, (d) DFSN, and (e) HABI.

these mechanophores have been introduced into polymer chains mainly by click reactions where heating is not usually required [114, 115]. To tackle this issue, a more promising mechanophore with a higher thermal resistance has been reported. Difluorenylsuccinonitrile (DFSN), a homodimer of fluorenylacetonitrile (Scheme 1.8d), has been exploited as a radical-type mechanochromophore centered in poly(methyl methacrylate) (PMMA) that changed color from white to pink upon grinding [117]. A DFSN dibromide was used as a bifunctional initiator to synthesize DFSN-centered PMMA via atom transfer radical polymerization (ATRP) at 50 °C, where the central C—C bond in the DFSN moiety was retained intact during the

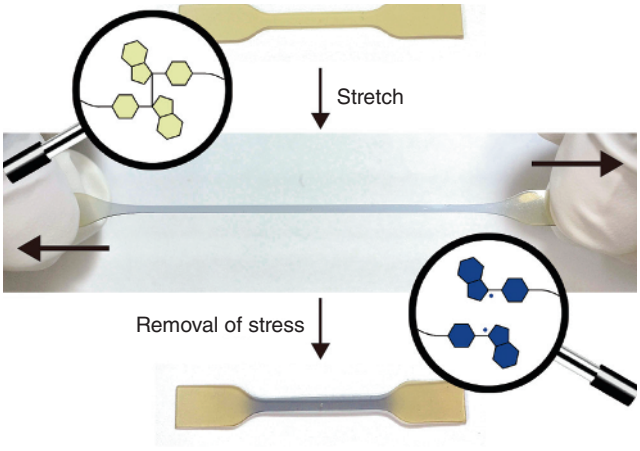

Figure 1.12 Optical images for manually stretched DABBF-linked polymer. Source: Reproduced with permission from Imato et al. [113]/American Chemical Society.

polymerization process. In this study, the DFSN-embedded polymer demonstrated superior thermal stability (e.g. the polymer did not show any color change even after heating to 150 °C).

A heteroatom-centered radical forming molecule is hexaarylbiimidazole (HABI) (Scheme 1.8e). The mechanical activation of mechanochromophore-embedded polymers has been reported to generate triphenylimidazolyl (TPI) radicals via the homolytic cleavage of central C—N bond of HABI moiety with a color change from yellow to green [118]. Here, the HABI units have been incorporated into the backbones of linear poly(methacrylate) and physically crosslinked polyurethane to show the mechanochemical activation of the HABI unit in solution state (via sonication) and solid state (via compression), respectively. Notably, this study demonstrated the use of mechanically generated TPI radicals to initiate radical polymerizations facilitated by sufficiently high amounts of a thiol-based chain transfer agent (e.g. methyl 3-mercaptopropionate).

In contrast to stable radical forming systems discussed above, we can find other heteroatom involved in weak dynamic covalent bonds, such as diselenides. These covalent bonds homolytically cleave to form radicals, which are not that stabilized. For example, ultrasound-induced selective scission of Se—Se bond-centered polystyrene chains has been reported, where the resulting polymeric selenium radicals could subsequently undergo metathesis reactions with an added small molecule comprising a diselenide functionality [119]. Osmotic pressure force-responsive rupturing of vesicles consisting of Se–Se-linked amphiphilic polymers has also been demonstrated, where a diselenide metathesis reaction was observed [120].

1.4.5 Other Types of Mechanophores

Any bond can break when the force is large enough, but polymer mechanochemistry deals with bond breakage that creates functionalities. In this section, we will

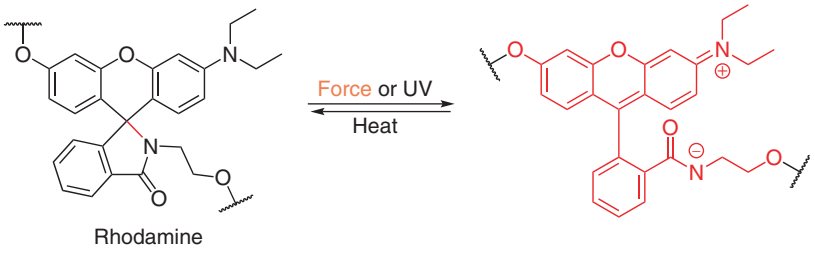

Scheme 1.9 Electrocyclic ring opening of rhodamine.

briefly describe mechanophores, including rhodamine, Bz, and dioxetane, that do not fall within any of the above categories. They offer unique optical properties upon mechanoactivation. Rhodamine is a fluorescent dye that undergoes isomerization from its ring-closed twisted spirolactam form to a ring-open planarized zwitterionic form via the cleavage of C_{spiro}—N bond, as shown in Scheme 1.9. Rh–OH was covalently linked to a polyurethane network. When the polymer was scratched using a pen-like pestle, only the scratched region turned red, demonstrating the mechanochromism of Rh–OH mechanochromophore via its stress-induced isomerization [121]. The color and fluorescence intensity of polymeric Rh–OH were studied as a function of the applied stress. Initially, a fluorescence emission band at 440 nm was observed with a blue color, and later a band at 550 nm emerged with a red color whose intensity increased with increasing applied stress. Importantly, fluorescence intensity remained invariant for the polymer control without Rh–OH. Apart from that, the fluorescence remained the same before and after applying force for samples containing blended crosslinked polymer and Rh–OH, further corroborating the stress-induced isomerization of Rh–OH in the embedded polymer. The color change observed in the polymer material was thermally reversible. It should be noted that this particular system was mechanically inactive for tensile stress.

Ultrasonication-induced Bz-appended aliphatic esters have been reported as a new class of photoluminescent mechanofluorophores [122]. In this study, because of the cleavage of relatively weak ester's C—O bond, the PMA-embedded Bz aliphatic ester (blue) mechanophore formed the free Bz, which has green photoluminescence (Scheme 1.10). The aliphatic ester of Bz emits blue light. This luminescence was a result of intramolecular proton transfer taking place from the electronic excited state. Unlike aromatic esters, the aliphatic ester groups make the polymer embedded mechanophores emissive. Therefore, the mechanoresponsiveness was not simply a turn-on or -off effect, yet a change in photoluminescence color. Here, gel-permeation chromatography (GPC) was used to monitor that mechanical activation indeed took place from the Bz moiety embedded in the PMA material, as shown in Figure 1.13.

Bis(adamantyl)-1,2-dioxetane mechanoluminophore-functionalized polymers exhibit ultrasonication and tensile stress-induced autochemiluminescence in solution and bulk materials, respectively [123]. Under the mechanical force, the ring opening of strained, four-membered 1,2-dioxetane generated two ketones of which one was in the electronic excited state, which emitted blue light (420 nm) as

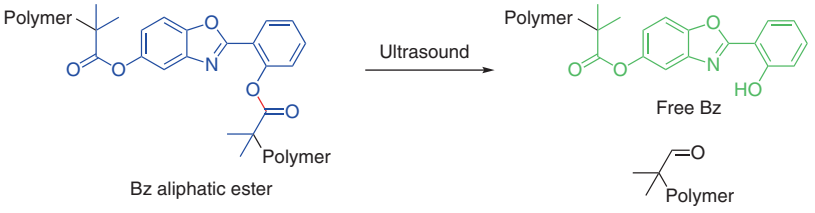

Scheme 1.10 Force-induced cleavage of benzoxazole aliphatic ester.

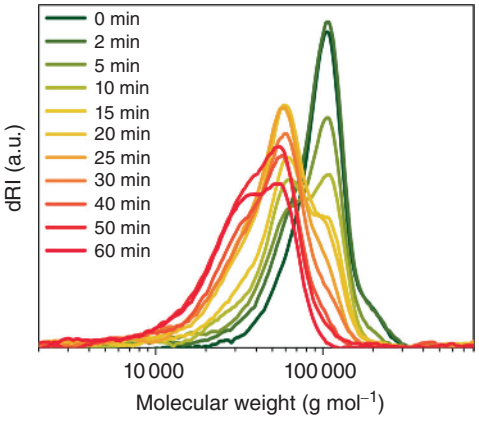

Figure 1.13 Representative GPC chromatograms of a PMA-Bz-PMA solution after ultrasonication at the indicated times. Source: Karman et al. [122]/with permission of American Chemical Society.

it relaxed to the ground state. It is possible to tune the emission color by transferring the excited-state energy to numerous acceptors [123, 124]. Here, the luminescence occurred in the absence of an excitation light source; meaning, it was exclusively the mechanical force that provided the necessary energy for the photon emission. Therefore, the use of conditions with minimal background signals is viable that in turn leads to improved sensitivity. The activation of 1,2-dioxetane permits for monitoring of bond scissions in real time with high tempo-spatial resolution. These mechanophores have been used as molecular damage indicators to map the damage regions in multiple network elastomers [125].

1.5 Polymer Noncovalent Mechanochemistry

When considering a covalent mechanophore, the bonds affected by mechanochemical stimuli are the weakest in the molecule [126]. Although the weakest in the system, the bond-dissociation energies are consistently hundreds of kilojoules per mole [127, 128]. These high-bonding energies, when reached by mechanochemical stimulation, do not favor spontaneous reformation. Lower energy noncovalent bonding systems, such as metal–ligand bonds, π-stacking, hydrogen bonding, and ionic interactions, feature shorter bond lifetimes, lower activation barriers, and the ability to readily re-associate upon removal of load and therefore should also be considered as mechanophores. Biological systems rely largely on noncovalent

interactions to control biomechanics. Synthetic polymer mechanochemistry has focused more on dissociable covalent bonds. However, mechanoresponses of secondary bonds offer unique functionalities due to fast dynamics and reversibility and have found applications in self-healing materials, mechanoenhancement of gels and elastomers, mechanochromism, and force-activated catalysts. Among them, metal–ligand bonds gained the most popularity. In many early studies, the metal–ligand bonds were observed to break following a mechanochemical stimulation [129]. Given the proper proximity of metal and the ligands, bonds can spontaneously form. The range of bond strengths can be tuned widely by both the identity and concentration of the metal and the ligand [130, 131]. Their maximum BDE can be near that of a covalent bond and down to that of a hydrogen bond [5]. Due to the tunability, metal–ligand bonds are the most studied noncovalent mechanophore and will be the main focus of discussion here.

1.5.1 Mechanoresponses of Metal–Ligand Bonds

Ferrocene (FC) has been studied to have high mechanical activity [132]. Initial accounts of ferrocene mechanochemistry in a polymer matrix demonstrated iron(III) ion (Fe^{3+}) liberation following ultrasonication [133]. The liberation of the Fe^{3+} induced a color change of a potassium thiocyanate solution from clear to red. This demonstrates the ability of ferrocene mechanopolymers to be mechanochromic. Sensitivity of ferrocene mechanopolymers is improved through the use of a conformational lock [134]. The "lock" covalently connects the ferrocene's cyclopentadienyl rings together through a hydrocarbon chain. The connection allows the metallopolymer to respond to mechanical force without initial rotation around the central ligand–metal–ligand axis. This lowers the force needed to liberate the Fe^{2+} while increasing the rate of liberation (Figure 1.14a). The conformational lock can vary in the number of atoms as well as cis or trans conformation of the anchoring points. (Figure 1.14b-1). Both cis and trans conformations were locked by a three-atom chain to determine the effects of conformation, while a five-atom chain locked only cis conformation to determine the dependence of chain strain on dissociation energy. As shown in Figure 1.14b-2, the least force for dissociation occurred at ~800 pN in the *cis*-ferrocenophane with a three-carbon conformational lock (*cis*-3FCP). The most force (1140 pN) was required for the same three-atom lock but in the trans position, indicating the critical role of anchoring points in force transduction. Furthermore, the cis conformational lock containing five atoms requires a greater force (960 pN) than its three-atom lock counterpart, indicating that increased strain provided by fewer atom locks is beneficial. Cis conformations were also determined to have the lowest dissociation rates, nearly 7 orders of magnitude faster than ferrocene without conformation locks (Figure 1.14b-3). A heavy object is dropped from a fixed distance onto a polydimethylsiloxane (PDMS) embedded with *cis*-3FCP to liberate Fe^{3+} (Figure 1.14c). The liberated ions can then complex with surrounding phenanthroline in the bulk polymer matrix, resulting in a color change of the bulk material from yellow to red orange. The color change of a covalently embedded

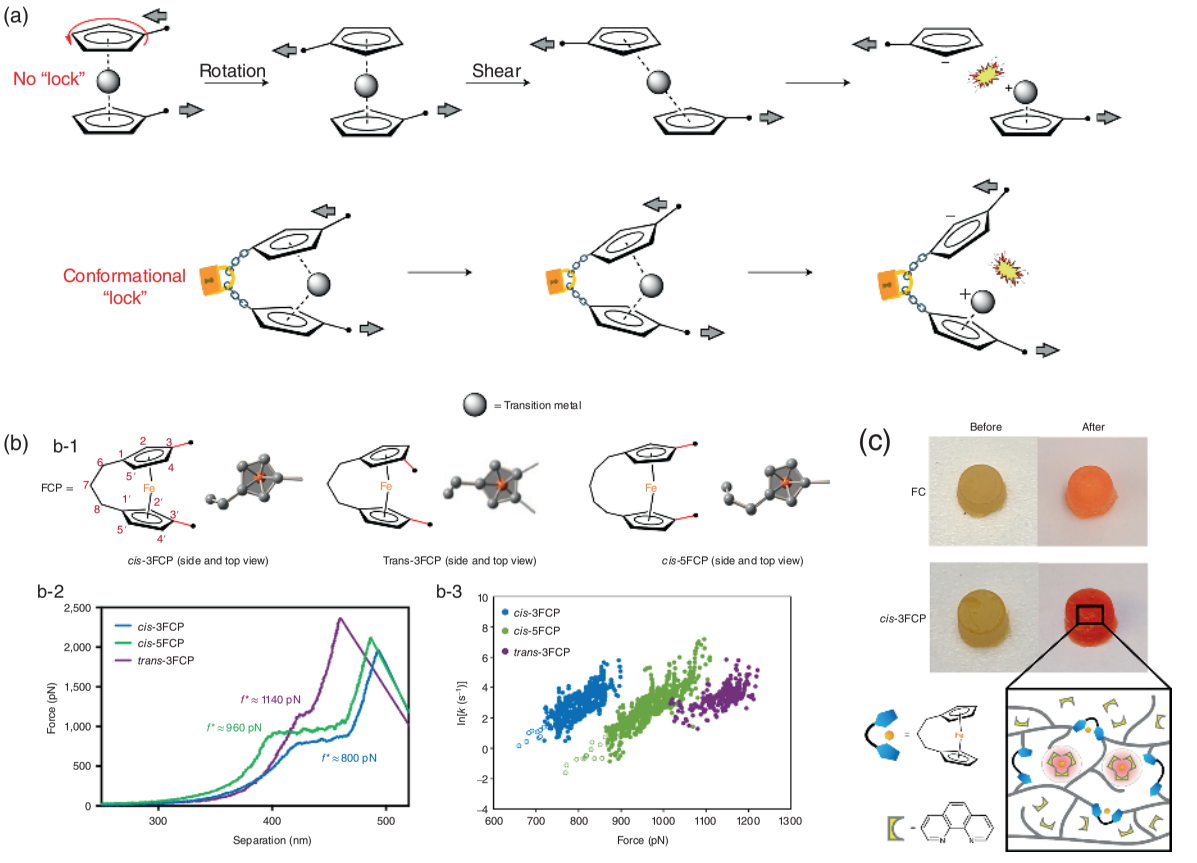

Figure 1.14 (a) Schematic of mechanochemical dissociation resulting in the Fe^{3+} liberation in unconstrained ferrocene and conformationally locked ferrocene. (b) The rate–force plot demonstrating the lowest energy Fe^{3+} liberation occurs in the cis conformation locked with a three-atom "lock" (*cis*-3FCP, blue). (c) Color of PDMS plug functionalized with *cis*-3FCP or unconstrained ferrocene (FC) before and after drop test (top) and schematic of phenanthroline-capturing liberated Fe^{3+} (bottom). Source: Reproduced with permission from Zhang et al. [134]/Springer Nature.

ferrocene (FC) without a conformation lock is less intense, from yellow to light orange. This confirms that unconstrained ferrocene results in fewer Fe^{3+} being liberated from ferrocene under the same force. However, this mechanochromism is irreversible because the cyclopentadienyl rings can dimerize by a Diels–Alder reaction to establish a covalent crosslinking, and the bonds between phenanthroline and Fe^{2+} are relatively stable. But the study demonstrated a promising approach to tune molecular mechanosensitivity.

Metal–ligand mechanopolymers are being widely implemented as catalysts. They can exist within a substrate in the latent state for extended periods of time until activated by stimuli [135]. Through ultrasound sonication, mechanocatalysts experience mechanically induced ligand dissociation, resulting in a switch to a coordinatively unsaturated active catalyst. The activated catalyst can then enter the catalytic cycle to perform the desired reaction. A polymetric ruthenium-based Grubbs-type olefin metathesis catalyst has been reported to induce ROMPs and ring-closing metathesis (RCM) [136]. The mechanically activated catalyst is based on a ruthenium alkylidene complex containing two *N*-heterocyclic carbene (NHC) ligands, which is known as a thermal latent catalyst [137]. It is then modified with polymer chains attached to the NHC ligands to afford a mechanocatalyst. Scheme 1.11 shows the ultrasonic scission of the mechanocatalyst to yield the active catalyst. The metal–ligand bond dissociation is more effective when the attached polymer chains are of higher molecular weight. This is demonstrated through the catalyzed RCM of diethyldiallyl malonate achieving 40% conversion using a high-molecular-weight polymer catalyst compared to 1% conversion using a low-molecular weight, given the same sonication time. Discontinuing ultrasonication is shown to immediately stop the catalyzed RCM, indicating limited lifetime of the active catalyst for that reaction. However, catalyzed ROMP has

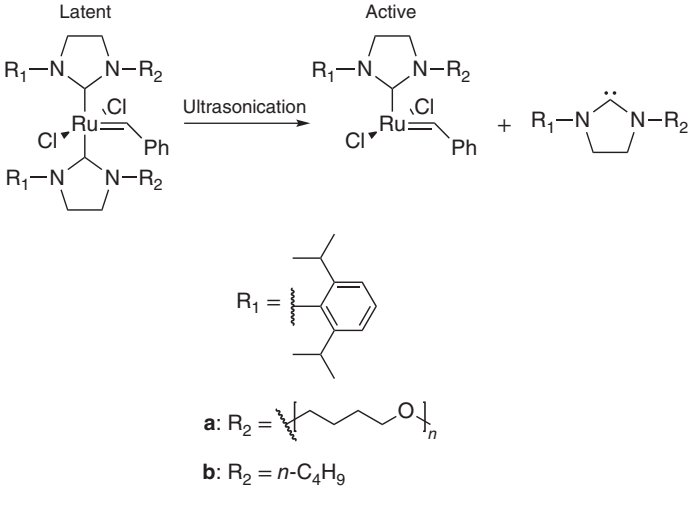

Scheme 1.11 Ultrasonic scission of latent mechanocatalyst to yield the active catalyst. Source: Piermattei et al. [136]/with permission of Springer Nature.

shown to continue hours following ultrasonication has stopped. This difference is consistent with other ROMP and RCM thermal catalysts [138]. Metal–ligand mechanopolymers have also been implemented as drug-delivery devices. Schmidt and coworkers discussed the mechanochemically activated drug delivery from an octahedral Pd cage [139]. All six vertexes contained a polyethylene glycol ($n = 220$)-decorated bipyridine to assemble the octahedral $Pd^{II}_6(TPT)_4$ cage around one molecule of ibuprofen. Upon ultrasound stimulation, the polymer chains experienced enough force to dissociate the Pd-2,4,6-tris(4-pyridyl)-1,3,5-triazine (TPT) metal–ligand bond. This resulted in cage fragmentation and subsequent release of pharmaceutically active cargo.

The presence of metal–ligand bonds, along with their dynamic dissociation and reassociation under mechanical forces, can significantly affect the mechanical properties of polymers. A recent example of a highly elastic self-healable material utilizes a dynamic tridentate 2,6-pyridinedicarboxamide ligand (pdca) on a PDMS polymer chain and complexed it with an Fe^{3+} transition metal (Figure 1.15a) [140]. Pdca contains three different atoms that can bind to the Fe^{3+} transition metal center with varying strengths. The order of the strongest to weakest bonds to Fe^{3+} is $N_{pyridine}$, N_{amide}, and O_{amide} verified by calculations using known valence parameters [141]. The transition metal center can bind to two pdca ligands allowing for interchain and intrachain crosslinking. The binding energies were verified

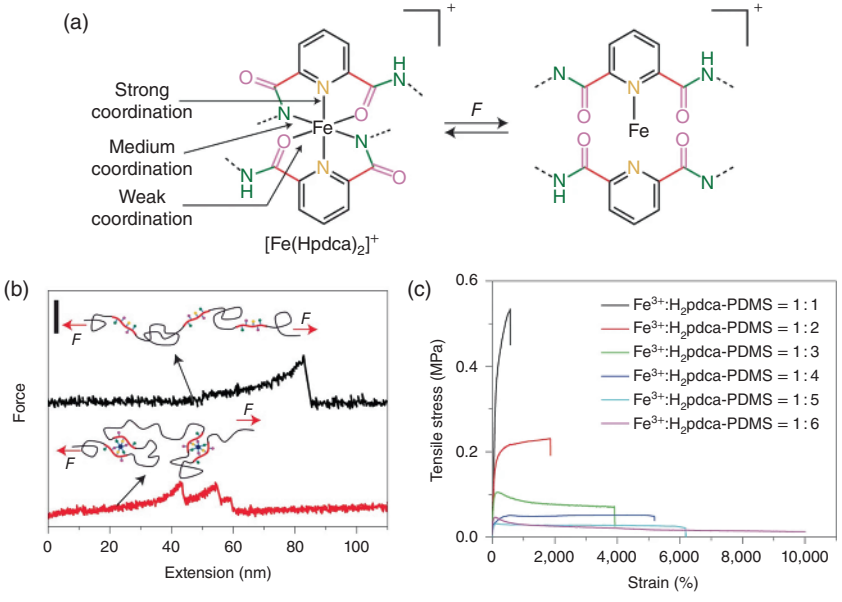

Figure 1.15 (a) Dynamic bonds pdca ligand to Fe^{3+} metal center that individually disconnects following input of mechanical force. (b) Force–extension curve that demonstrates one high-energy bond breakage before addition of Fe^{3+} (black) and three individual bond breakages following addition of Fe^{3+} ligand crosslinks (red). (c) Stress–strain curves demonstrating the dependence of Fe^{3+} concentration to pdca ligand for strength and elasticity. Source: Li et al. [140]/with permission of Springer Nature.

by a force–extension curve measured via single-molecule force spectroscopy (Figure 1.15b). The force–extension curve of a linear pdca–PDMS chain shows a single rupture at 80 nm, signifying a nonspecific covalent bond dissociation. When $FeCl_3$ is added to the linear pdca–PDMS chain, intramolecular crosslinking occurs. This results in a force–extension curve containing three individual bond dissociations (Figure 1.15b). Each of the dissociations is attributed to the three unique bonding energies of the atoms within the tridentate ligand. The covalent rupture no longer appears at 80 nm, suggesting a stabilization of the polymer backbone due to force dissipation metal–ligand bond dissociation. As the material is stretched, the dynamic bond strengths result in controlled bond dissociation, instead of harsh rupture. When all three metal–ligand bonds are broken, the chain slides allowing nonbonded pdca to be in a favorable position to attach to a newly available transition metal center. This strengthens the molecule as it stretches, allowing for further stretching without material failure. Due to these metal–ligand interactions, this material can be stretched beyond 10 000% of its original length with a relatively low Fe^{3+} concentration. The higher concentration of Fe^{3+} increases the crosslink density, resulting in a material with high tensile strength (Figure 1.15c). The dynamic breaking and reforming of metal–ligand bonds during mechanical deformation of a bulk material can be probed using nonlinear rheology [142, 143]. It complements the single-molecule force spectroscopy and provides insights on bond mechanosensitivity in highly anisotropic force environments within highly coiled and entangled systems. For the material shown in Figure 1.15a, rheology measurements confirmed the chain extensions and alignments when the shear rate is much higher than chain relaxation rate, allowing metal–ligand bonds to reform after extension cessation at high strains. Materials that exhibit high stretchability can also exhibit self-healing capabilities [144–146]. When the material was cut and placed back together for 48 hours at room temperature, it could stretch to 90% of what the uncut material could achieve. When allowed to self-heal at −20 °C for 72 hours, it could stretch 68% of an uncut material. This is reported as the first autonomous self-healing material at such low temperatures without additional stimuli.

Transition metals can vary in coordination number, ionic radius, and oxidation state. Thus, mechanical properties differ between two metallopolymers composed of the same ligands but crosslinked with different metals. Monodentate imidazole containing polymers (ICPs) have shown variation in mechanical properties, such as Young's modulus and ultimate extensibility, when crosslinked to different metal centers (Figure 1.16a,b) [147]. In this case, the metals analyzed were Co^{2+} and Zn^{2+}, which are similar in ionic radius and oxidation but differ in coordination number. The coordination numbers of Co^{2+} and Zn^{2+} are six and four, respectively. The crosslink density can be easily tuned by changing the ligand-to-metal ratio (L/M). As expected, increase in metal concentration resulted in higher Young's modulus (E) due to a higher crosslink density. However, the ultimate extensibility (ε_{ult}) is not exclusively related to crosslink density. Rather it is based on metal–ligand-exchange kinetics. The ε_{ult} for zinc does not significantly change when the L/M concentration is reduced from 8 to 4.5. This indicates fast ligand-exchange kinetics. However,

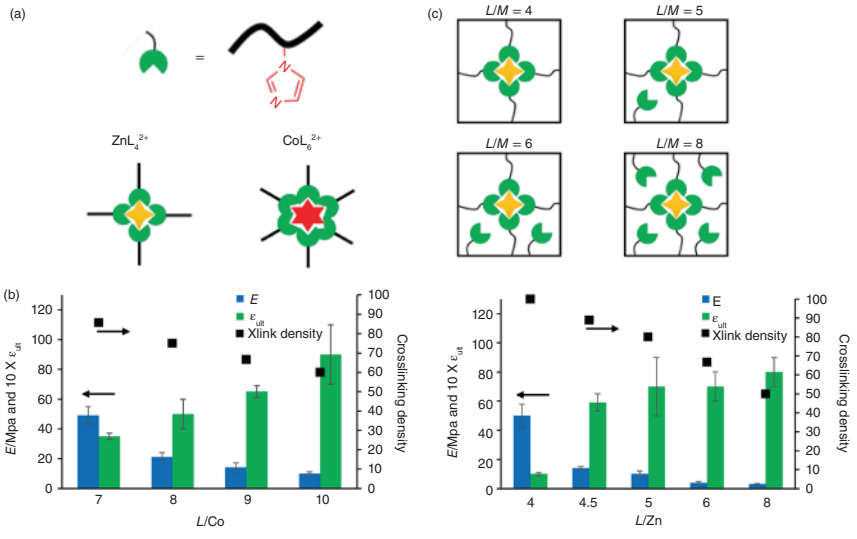

Figure 1.16 (a) Schematic of imidazole ligand binding to zinc (yellow) and cobalt (red) metal centers. (b) Comparison of Young's modulus (E) and ultimate extensibility (ε_{ult}) for various concentrations of ICP crosslinked to cobalt (left) and zinc (right). (c) Schematic of imidazole-zinc ligand exchange in the presence of increasing concentration of ligand. Source: Mozhdehi et al. [147]/with permission of Springer Nature.

when L/Zn decreases to 4, Zn's coordination number, ε_{ult} decreases significantly as there are not any available ligands to exchange, causing the polymer to stiffen (Figure 1.16c). Considering the ε_{ult} of Co, there is a consistent decrease with decreasing L/Co. This suggests concentration-dependent, slow ligand-exchange kinetics. The L/M crosslinks behave more like covalent bonds. If the L/Co reduces to Co's coordination number, one would expect another substantial decrease in ε_{ult}, which is not observed experimentally. The difference in ligand-exchange rates originates from their coordination number and transition states. In the presence of excess ligands, Co^{2+} prefers to form octahedral complexes. Because of the steric hindrance of the octahedral complex, it undergoes dissociative ligand exchange. In comparison, Zn^{2+} prefers complexes with a lower coordination number; therefore, ligand exchange proceeds through associative pathways. Ligand-exchange kinetics directly controls the molecule's ability to self-heal. Zn ICP experiences complete recovery of Young's modulus after 3 hours of room-temperature healing, while Co ICP only experiences ~50% recovery after 24 hours of healing.

Hydrogels have broad applications in biomedical fields, but they often suffer from poor mechanical strengths. The presence of noncovalent interactions significantly enhances the strength, stretchability, and toughness of hydrogels as in bulk polymers due to their dynamics under stress or strain. This has been demonstrated in a double-network gel composed of polyacrylamide (PAA) and alginate crosslinked by three different types of bonds (Figure 1.17a) [148]. The alginate chain comprises mannuronic acid (M blocks) and guluronic acid blocks (G blocks). The G blocks can form the ionic crosslinks in the presence of a divalent cation, such as Ca^{2+}. The M

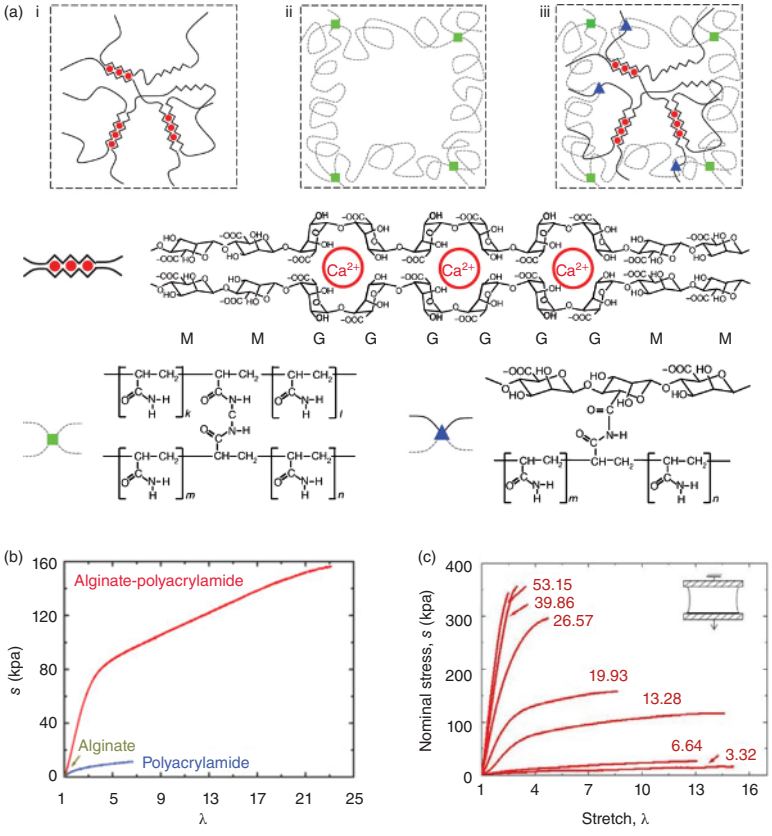

Figure 1.17 (a) Schematic of (i) ionic crosslinks between alginate chains in the presence of Ca^{2+}, (ii) covalent crosslinks between PAA chains, (iii) covalent crosslinks between alginate and PAA. (b) Stress–stretch curves of individual components, alginate, and PAA compared to the hybrid hydrogel. (c) Stress–stretch curves of weight ratios of $CaSO_4$ to alginate, as labeled. Source: Sun et al. [148]/with permission of Springer Nature.

block contains a carbonyl which covalently crosslinks with the amide in PAA in the presence of a *N*,*N*-methylenebisacrylamide crosslinker. Meanwhile, the PAA is also covalently crosslinked. The hybrid gel of these two components can stretch much further and withstand much more stress than as individuals (Figure 1.17b). The enhanced elasticity is attributed to the load sharing of both alginate and PAA chains. As mechanical force increases, the bonds between the Ca^{2+} ions and the G blocks unzip progressively, while the covalent crosslinks remain unbroken. Selective breaking of ionic crosslinks allows for force dissipation without complete material failure. When Ca^{2+} is present around free G blocks, they can rebind to stabilize the gel as it is stretched. The tensile strain (λ) of the hydrogel decreases with increasing Ca^{2+} concentration, but the tensile stress increases (Figure 1.17c). Given water's role in a hydrogel, many diminish in stretchability and toughness below their freezing point at 0 °C; however, the increased concentration of calcium salts induces freezing-point depression which allows for low-temperature mechanoactivity [149]. When soaked

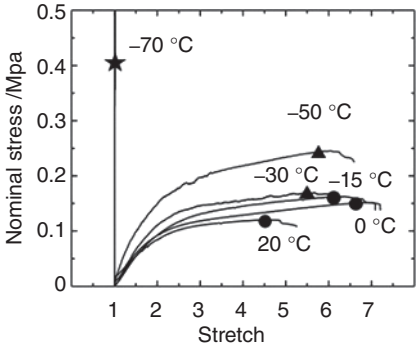

Figure 1.18 Stress–stretch curves of PAA-alginate hydrogel in 30 wt% $CaCl_2$ solution under reduced temperature. Circles are regular hydrogels, triangles are slurry gels, and stars are frozen gels. Source: Morelle et al. [149]/with permission of John Wiley & Sons.

in a 30 wt% $CaCl_2$ solution and temperature is reduced below −30 °C, the hydrogel transforms into a "slurry gel" (Figure 1.18). A slurry gel's increase in toughness is attributed to the formation of ice crystals. The ice crystals increase the volume fraction of the gel, allowing deformation to occur by a stronger shear yielding between them. More remarkably, stretchability also increases due to the formation of microcavities. The microcavities nucleate at the interface between ice crystals and the liquid saltwater solution, which provides a new force dissipation mechanism, resulting in enhanced stretchability.

1.5.2 Mechanochemistry of Other Noncovalent Interactions and Their Applications in Functional Polymers

The development of polymer mechanochemistry is largely driven by the opportunity to create new functional materials. One of the most extensively studied is self-healing polymers. Dynamic breaking and reformation of noncovalent interactions under mechanical force can effectively enhance material strength and lower the activation energy for self-healing to take place. Most noncovalent interactions, including metal–ligand bonds, hydrogen bonding, ionic interactions, π–π stacking, host–guest interactions, and van der Waals forces, have been utilized. The inspiration comes from the healing ability of natural tissue. If materials are capable of sensing and repairing damages on their own, their performance and lifetime will be greatly enhanced.

Noncovalent interactions enable autonomous healing by playing dual roles. One is that they enable healing by breaking and reforming bonds. When the material is mechanically damaged, the noncovalent bonds break, creating nonbonded motifs at the freshly cut surface. When the damaged parts are in contact, chains diffuse and randomize while noncovalent bonds reform, thus erasing the interface and restoring the original material properties. In this case, the healing efficiency is dependent on the resting time from the time the cut is made till the contact is generated. If the bonds undergo fast thermal fluctuations (spontaneous regime, Figure 1.8), self-healing is less dependent on mechanical scission and resting time. The fast dynamics can allow self-healing at temperatures as low as −40 °C [140, 150]. The other role that noncovalent interactions play is providing viscoelastic

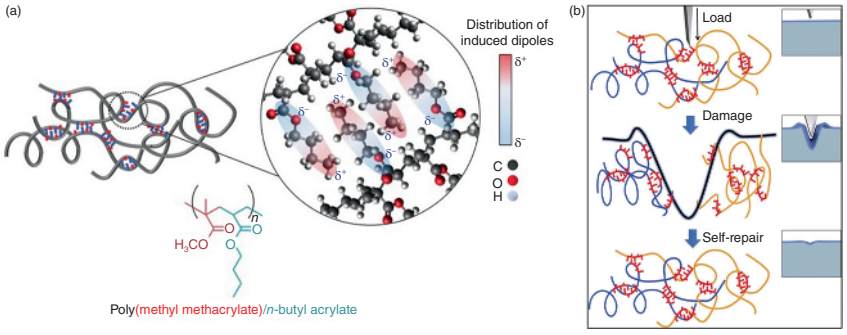

Figure 1.19 Schematic illustration of (a) key-and-lock interaction of poly(methyl methacrylate-*co*-*n*-butyl acrylate) and (b) the self-healing of a scratch driven by both network elasticity and reformation of key-and-lock interactions. Source: Urban et al. [151]/with permission of AAAS.

properties that are favorable for self-healing. This was demonstrated in a study that utilized weak van der Waal interactions to enable self-healing of simple commodity polymers [151]. Although individual van der Waals interaction is extremely weak, the collective force of many of these bonds significantly affects the viscoelasticity of the bulk polymer, similar to small molecules for which intermolecular forces determine many of their physical properties. In this study, commodity copolymers of methyl methacrylate and *n*-butyl acrylate were shown to have favorable interchain van der Waals forces that form key-and-lock interchain junctions within certain compositional range (Figure 1.19). The interaction was attributed to the polarity of the poly(butyl acrylate) pendant groups and a favorable steric environment formed by copolymerizing with the methyl methacrylate. As a result, cohesive energy density increased, and the material gained sufficient elasticity so that chains underwent elastic deformation instead of slippages during mechanical damage, storing the mechanical energy. Upon force removal, the cut then closed on its own by entropy-driven elastic recovery. Copolymer chains returned to their initial conformations in a spring-like manner. Meanwhile, fast dynamics of the van der Waals forces allowed chains to randomize at the interface on a longer time scale and reform key-and-lock junctions.

In this example, the collective force of noncovalent interactions seems to inhibit bond breaking during damage, contradicting the common conception that their breaking and reforming dynamics are responsible for healing. However, it is the favorable thermodynamic and kinetic characteristics within the material that drive the self-healing processes. The change of chain morphologies, increased entanglements, force transduction, and viscoelasticity affected by noncovalent interactions should be taken into consideration in addition to the bond dynamics when considering the self-healing mechanisms. Covalent bonds may also break during damage unless the chains slip out before breaking. Mending of covalent bonds is done through thermal or photo-reversible reactions. Despite the importance of mechanochemistry in self-healing materials, many studies do not offer evidence as to what bonds break at the site of damage and how they contribute

to the recovery. However, the amount of chemistries that have been utilized in mechanoresponsive self-healing materials is tremendous and can be found in many comprehensive reviews [152–156].

There have been increasing numbers of studies that utilize noncovalent mechanochemistry to develop functional materials beyond self-healing in recent years. One of such applications is drug activation by ultrasound-induced scission of mechanosensitive noncovalent bonds [70]. When a drug is complexed to a substrate via noncovalent interactions, it is deactivated. The hypothesis is thus that if ultrasound can break the interactions, the drug can then be freed from the substrates and become activated to bind to the target. In the work by Huo et al., two systems were developed based on this hypothesis. One relies on the strong binding of RNA aptamers to their targets (Figure 1.20a). The RNA aptamer used here is R23, which selectively binds to aminoglycoside antibiotics, including neomycin B and paromomycin via non-covalent interactions, such as hydrogen bonds or electrostatic interactions. Once bound to the aptamer, these drugs are deactivated. To make the complex mechanically cleavable, the authors incorporated R23 aptamer units into high molar mass RNA strands followed by loading of the antibiotics. It was found that ultrasonication destroyed the noncovalent interactions between the drug and the aptamer. Additionally, covalent bond scission of the phosphodiester RNA backbone was observed. Ultimately, antimicrobial properties of the drugs were activated by 30 minutes of ultrasound treatment. In comparison, the same drugs loaded to just the aptamers, which are oligonucleotide sequences, did not respond to ultrasonication because of the short-chain length. Another approach developed by the authors was based on force-sensitive prodrug assemblies. The supramolecular binding between vancomycin (Van) with its H-bond-complementary peptide target sequence Cys-Lys-Lys(Ac)-d-Ala-d-Ala (DADA) was used as a proof of concept. As shown in Figure 1.20b, to obtain sufficient force sensitivity, this supramolecular motif was incorporated between poly(oligo(ethylene glycol) methyl ether methacrylate) (POEGMEMA) polymer chains and gold nanoparticles (AuNPs), or between two AuNPs. For both systems, selective mechanochemical scission of the H-bonded motif occurred, leading to successful activation of the antimicrobial drug Van toward *Staphylococcus aureus*. The concept was also successfully extended to ultrasound-induced activation of enzyme activity [157].

Host–guest interactions are highly dynamic in aqueous environments. Therefore, they have been widely used in stimuli-responsive hydrogels [158, 159]. Recently, the use of β-cyclodextrin (host) and adamantane (guest) complex to develop mechanoresponsive hydrogels has been explored. An approach by Hippler et al. utilized a small-molecule competitive guest, adamantanecarboxylic acid, to control the material's force responses [160]. Both host and guest moieties were attached to acrylamide backbone that formed a rigid hydrogel following host–guest crosslinking. Addition of a solution containing the competitive guest decreased the crosslink density as the competitive guest began to occupy host sites. This resulted in a softer hydrogel. Under the same applied force, the competitive guest containing hydrogel was reported to experience a greater deformation than the hydrogel without the competitive guest. A different approach by Uyama and

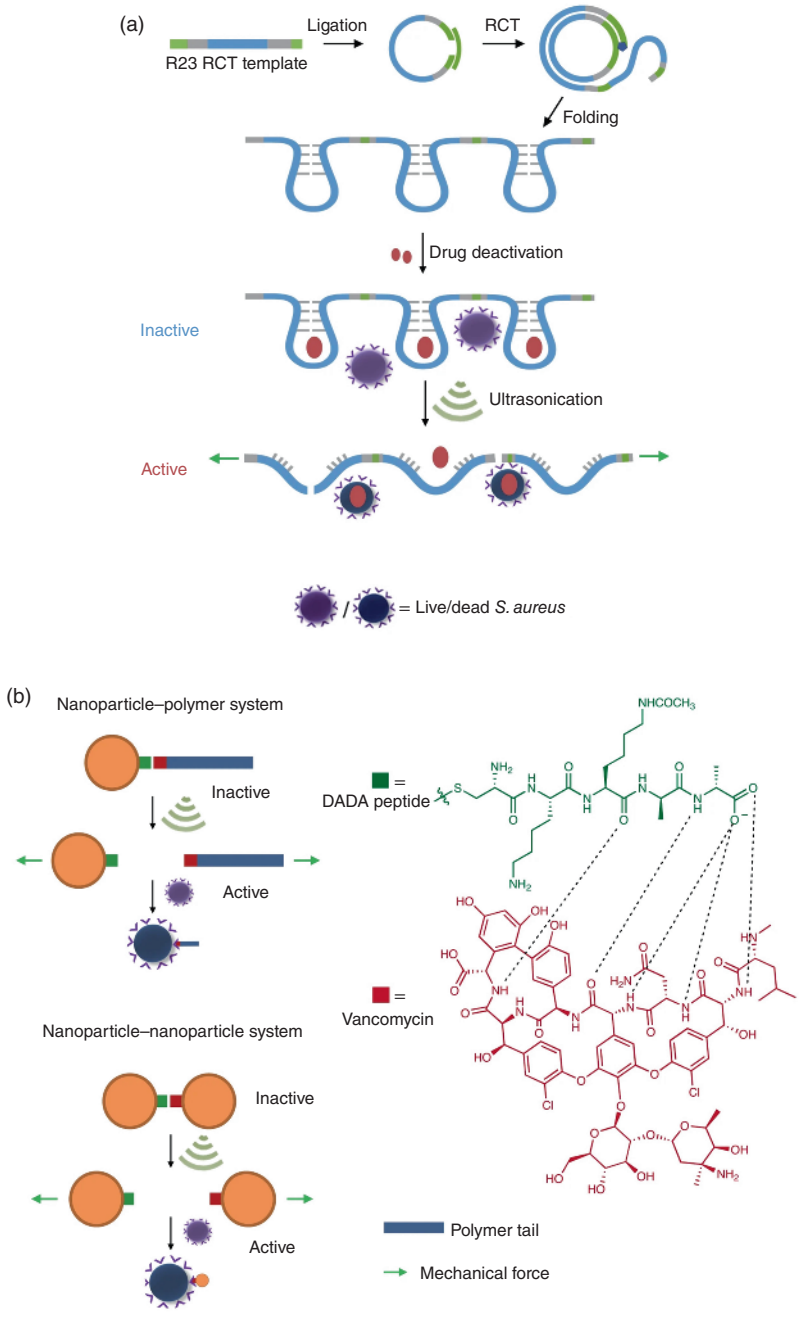

Figure 1.20 Design principle for drug activation by ultrasound scission of noncovalent bonds. (a) Synthesis of polyaptamers R23 via rolling-circle transcription (RCT), drug loading, and subsequent activation and release of the drug by ultrasound to kill *S. aureus* bacteria. (b) Mechanoactivation of nanoparticle–polymer and nanoparticle–nanoparticle assemblies via breaking the H-bonding between DADA–vancomycin pairs to activate the antibiotic properties of the vancomycin drug. Source: Huo et al. [70]/with permission of Springer Nature.

coworkers utilized a hydrogel comprising an adamantane containing thermoresponsive polymer and β-cyclodextrin containing non-thermoresponsive network to afford a stimuli-responsive phase transition [161]. The phase transition of the poly(*N*-isopropylacrylamide) thermoresponsive polymer was restricted even above its lower critical solution temperature (LCST) because of its host–guest connection to the non-thermoresponsive network. Following applied mechanical stress, the host–guest interactions dissociate, and the coil–globule transition typical of the thermoresponsive polymer above its LCST occurred. The hydrogel became opaque following compression, quantified by a decrease in transmittance. Cooling the hydrogel below LCST redistributed the thermoresponsive polymer within the network, regaining original transparency.

1.6 Conclusions

Mechanochemistry plays an indispensable role in many complicated biological processes from cellular growth to repair; however, the design of comparable abiotic mechanical systems that are as sophisticated as nature remains challenging. Over the past decade, synthetic mechanoresponsive materials have attracted immense attention for their numerous practical applications and unique reactivity that is simply not feasible with thermo- or photochemistry. The emergence of new tools to gain more insight into mechanisms of mechanochemical reactions has sparked increasing curiosity in the field. In this chapter, the unique mechanisms of mechanochemistry are discussed followed by introduction of various covalent and noncovalent mechanoactive bonds. By incorporating these bonds into polymers, materials with functionalities, including stress sensing, self-healing, release of small molecules, such as catalysts or drugs, stress mitigation, creation of tougher and stronger materials, and mechanoactivation of smart functionalities, can be created. The ubiquitous energy difference between covalent and noncovalent bonds allows for a wide variety of molecular compositions to experience selective force-induced bond dissociations. Covalent mechanochemistry has undergone more extensive studies, while noncovalent interactions will continue to play an important role in synthesizing functional mechanopolymers. Polymer materials functionalized with mechanophores that are based on drug molecules will find applications in the biomedical field which are shown in recent studies using covalent mechanophores or supramolecular assemblies [69, 162]. Future developments will take inspiration from new chemistries to improve on current strength, stretchability, and self-healing to exhibit properties that emulate biological tissues [163–166]. When specifically considering muscle tissue, adding electrically conductive functionality to mechanopolymers will be the next step in achieving materials that closely match complete tissue function [145, 167–170]. Creating sensing and signaling pathways similar to bio mechanotransduction will allow future materials to be adaptive to the mechanical environment to perform vital functionalities.

References

1 Takacs, L. (2013). The historical development of mechanochemistry. *Chem. Soc. Rev.* 42 (18): 7649–7659.
2 Takacs, L.M. (2004). Carey Lea, the first mechanochemist. *J. Mater. Sci.* 39 (16): 4987–4993.
3 Ostwald, W. (1919). Die Chemische Literatur Und Die Organisation Der Wissenschaft. In: *Handbuch Der Allgemeinen Chemie*. Gesel.: Akad. Verlag. m. b. H. 1–120.
4 IUPAC In Compendium of Chemical Terminology (1997). 2nd ed. (the "Gold Book"). Compiled by A.D. McNaught and A. Wilkinson. Oxford: Blackwell Scientific Publications. Online version (2019) created by S.J. Chalk. ISBN 0-9678550-9-8. https://doi.org/10.1351/goldbook.
5 Baláž, P., Achimovičová, M., Baláž, M. et al. (2013). Hallmarks of mechanochemistry: from nanoparticles to technology. *Chem. Soc. Rev.* 42 (18): 7571–7637.
6 Akbulatov, S. and Boulatov, R. (2017). Experimental polymer mechanochemistry and its interpretational frameworks. *ChemPhysChem* 18 (11): 1422–1450.
7 Willis-Fox, N., Rognin, E., Aljohani, T.A., and Daly, R. (2018). Polymer mechanochemistry: manufacturing is now a force to be reckoned with. *Chem* 4 (11): 2499–2537.
8 Hu, H., Ma, Z., and Jia, X. (2020). Reaction cascades in polymer mechanochemistry. *Mater. Chem. Front.* 4 (11): 3115–3129.
9 Izak-Nau, E., Campagna, D., Baumann, C., and Göstl, R. (2020). Polymer mechanochemistry-enabled pericyclic reactions. *Polym. Chem.* 11 (13): 2274–2299.
10 Abi Ghanem, M., Basu, A., Behrou, R. et al. (2020). The role of polymer mechanochemistry in responsive materials and additive manufacturing. *Nat. Rev. Mater.* 6: 84–98.
11 O, Neill, R.T. and Boulatov, R. (2021). The many flavours of mechanochemistry and its plausible conceptual underpinnings. *Nat. Rev. Chem.* 5 (3): 148–167.
12 Chen, Y., Mellot, G., Van Luijk, D. et al. (2021). Mechanochemical tools for polymer materials. *Chem. Soc. Rev.* 50 (6): 4100–4140.
13 Tsimbouri, P. (2015). Adult stem cell responses to nanostimuli. *J. Funct. Biomater.* 6 (3): 598–622.
14 McNamara, L.E., Burchmore, R., Riehle, M.O. et al. (2012). The role of microtopography in cellular mechanotransduction. *Biomaterials* 33 (10): 2835–2847.
15 Majkut, S., Dingal, P.C.D.P., and Discher, D.E. (2014). Stress sensitivity and mechanotransduction during heart development. *Curr. Biol.* 24 (10): R495–R501.
16 Ucar, H. and Kasai, H. (2021). Forceful synapses reveal mechanical interactions in the brain. *Nature* https://doi.org/10.1038/d41586-021-03516-0.
17 Lavalle, P., Boulmedais, F., Schaaf, P., and Jierry, L. (2016). Soft-mechanochemistry: mechanochemistry inspired by nature. *Langmuir* 32 (29): 7265–7276.

18 Collier, J.H., Rudra, J.S., Gasiorowski, J.Z., and Jung, J.P. (2010). Multi-component extracellular matrices based on peptide self-assembly. *Chem. Soc. Rev.* 39 (9): 3413–3424.

19 Chidanguro, T., Weng, W., and Simon, Y.C. (2018). Mechanochemistry: inspiration from biology. In: *RSC Polymer Chemistry Series*, Chapter 1, vol. 2018 (ed. Y.C. Simon and S.L. Craig), 1–35. Royal Society of Chemistry.

20 Okhota, S., Melnikov, I., Avtaeva, Y. et al. (2020). Shear stress-induced activation of von Willebrand factor and cardiovascular pathology. *Int. J. Mol. Sci.* 21 (20): 7804.

21 Crawley, J.T.B., De Groot, R., Xiang, Y. et al. (2011). Unraveling the scissile bond: how ADAMTS13 recognizes and cleaves von Willebrand factor. *Blood* 118 (12): 3212–3221.

22 Fogelson, A.L. and Neeves, K.B. (2015). Fluid mechanics of blood clot formation. *Annu. Rev. Fluid Mech.* 47: 377–403.

23 Zhang, Q., Zhou, Y.F., Zhang, C.Z. et al. (2009). Structural specializations of A2, a force-sensing domain in the ultralarge vascular protein von Willebrand factor. *Proc. Natl. Acad. Sci. U.S.A.* 106 (23): 9226–9231.

24 Holten-Andersen, N., Harrington, M.J., Birkedal, H. et al. (2011). PH-induced metal–ligand cross-links inspired by mussel yield self-healing polymer networks with near-covalent elastic moduli. *Proc. Natl. Acad. Sci. U.S.A.* 108 (7): 2651–2655.

25 Springer, T.A. (2011). Biology and physics of von Willebrand factor concatamers. *J. Thromb. Haemost.* 9: 130–143.

26 Harrington, M.J., Masic, A., Holten-Andersen, N. et al. (2010). Iron-clad fibers: a metal-based biological strategy for hard flexible coatings. *Science* 328 (5975): 216–220.

27 Hoffmann, T., Tych, K.M., Hughes, M.L. et al. (2013). Towards design principles for determining the mechanical stability of proteins. *Phys. Chem. Chem. Phys.* 15: 15767–15780.

28 Vélez-Ortega, A.C., Freeman, M.J., Indzhykulian, A.A. et al. (2017). Mechanotransduction current is essential for stability of the transducing stereocilia in mammalian auditory hair cells. *Elife* 6: e24661.

29 Lumpkin, E.A. and Caterina, M.J. (2007). Mechanisms of sensory transduction in the skin. *Nature* 445: 858–865.

30 Walsh, C.M., Bautista, D.M., and Lumpkin, E.A. (2015). Mammalian touch catches up. *Curr. Opin. Neurobiol.* 34: 133–139.

31 Hermans, T.M., Frauenrath, H., and Stellacci, F. (2013). Droplets out of equilibrium. *Science* 341 (6143): 243–244.

32 Hickenboth, C.R., Moore, J.S., White, S.R. et al. (2007). Biasing reaction pathways with mechanical force. *Nature* 446 (7134): 423–427.

33 Lenhardt, J.M., Black, A.L., and Craig, S.L. (2009). *gem*-Dichlorocyclopropanes as abundant and efficient mechanophores in polybutadiene copolymers under mechanical stress. *J. Am. Chem. Soc.* 131 (31): 10818–10819.

34 Lenhardt, J.M., Ong, M.T., Choe, R. et al. (2010). Trapping a diradical transition state by mechanochemical polymer extension. *Science* 329 (5995): 1057–1060.

35 Akbulatov, S., Tian, Y., and Boulatov, R. (2012). Force–reactivity property of a single monomer is sufficient to predict the micromechanical behavior of its polymer. *J. Am. Chem. Soc.* 134 (18): 7620–7623.

36 Ong, M.T., Leiding, J., Tao, H. et al. (2009). First principles dynamics and minimum energy pathways for mechanochemical ring opening of cyclobutene. *J. Am. Chem. Soc.* 131 (18): 6377–6379.

37 Kochhar, G.S., Bailey, A., and Mosey, N.J. (2010). Competition between orbitals and stress in mechanochemistry. *Angew. Chem. Int. Ed.* 49 (41): 7452–7455.

38 Wollenhaupt, M., Krupička, M., and Marx, D. (2015). Should the Woodward–Hoffmann rules be applied to mechanochemical reactions? *ChemPhysChem* 16 (8): 1593–1597.

39 Ribas-Arino, J., Shiga, M., and Marx, D. (2009). Understanding covalent mechanochemistry. *Angew. Chem. Int. Ed.* 48 (23): 4190–4193.

40 Bell, G.I. (1978). Models for the specific adhesion of cells to cells. *Science* 200 (4342): 618–627.

41 Hess, H. (2012). Optimal loading of molecular bonds. *Nano Lett.* 12 (11): 5813–5814.

42 Stauch, T. and Dreuw, A. (2016). Advances in quantum mechanochemistry: electronic structure methods and force analysis. *Chem. Rev.* 116 (22): 14137–14180.

43 Dammer, U., Hegner, M., Anselmetti, D. et al. (1996). Specific antigen/antibody interactions measured by force microscopy. *Biophys. J.* 70 (5): 2437–2441.

44 Smith, S.B., Cui, Y., and Bustamante, C. (1996). Overstretching B-DNA: the elastic response of individual double-stranded and single-stranded DNA molecules. *Science* 271 (5250): 795–799.

45 Hinterdorfer, P., Baumgartner, W., Gruber, H.J. et al. (1996). Detection and localization of individual antibody–antigen recognition events by atomic force microscopy. *Proc. Natl. Acad. Sci. U.S.A.* 93 (8): 3477–3481.

46 Oberhauser, A.F., Marszalek, P.E., Erickson, H.P., and Fernandez, J.M. (1998). The molecular elasticity of the extracellular matrix protein tenascin. *Nature* 393 (6681): 181–185.

47 Marszalek, P.E., Oberhauser, A.F., Pang, Y.-P., and Fernandez, J.M. (1998). Polysaccharide elasticity governed by chair–boat transitions of the glucopyranose ring. *Nature* 396 (6712): 661–664.

48 Grandbois, M., Beyer, M., Rief, M. et al. (1999). How strong is a covalent bond? *Science* 283 (5408): 1727–1730.

49 Wang, J., Kouznetsova, T.B., Niu, Z. et al. (2015). Inducing and quantifying forbidden reactivity with single-molecule polymer mechanochemistry. *Nat. Chem.* 7 (4): 323.

50 Wiita, A.P., Ainavarapu, S.R.K., Huang, H.H., and Fernandez, J.M. (2006). Force-dependent chemical kinetics of disulfide bond reduction observed with single-molecule techniques. *Proc. Natl. Acad. Sci. U.S.A.* 103 (19): 7222–7227.

51 Beedle, A.E.M., Mora, M., Davis, C.T. et al. (2018). Forcing the reversibility of a mechanochemical reaction. *Nat. Commun.* 9: 3155.

52 Pobelov, I.V., Lauritzen, K.P., Yoshida, K. et al. (2017). Dynamic breaking of a single gold bond. *Nat. Commun.* 8: 15931.

53 Evans, E. and Ritchie, K. (1997). Dynamic strength of molecular adhesion bonds. *Biophys. J.* 72 (4): 1541–1555.

54 Schönherr, H., Beulen, M.W.J., Bügler, J. et al. (2000). Individual supramolecular host–guest interactions studied by dynamic single molecule force spectroscopy. *J. Am. Chem. Soc.* 122 (20): 4963–4967.

55 Merkel, R., Nassoy, P., Leung, A. et al. (1999). Energy landscapes of receptor–ligand bonds explored with dynamic force spectroscopy. *Nature* 397 (6714): 50–53.

56 Friddle, R.W., Podsiadlo, P., Artyukhin, A.B., and Noy, A. (2008). Near-equilibrium chemical force microscopy. *J. Phys. Chem. C* 112 (13): 4986–4990.

57 Huang, Z., Xu, B., Chen, Y. et al. (2006). Measurement of current-induced local heating in a single molecule junction. *Nano Lett.* 6 (6): 1240–1244.

58 Ribas-Arino, J. and Marx, D. (2012). Covalent mechanochemistry: theoretical concepts and computational tools with applications to molecular nanomechanics. *Chem. Rev.* 112 (10): 5412–5487.

59 Beyer, M.K. (2000). The mechanical strength of a covalent bond calculated by density functional theory. *J. Chem. Phys.* 112 (17): 7307–7312.

60 Kean, Z.S., Gossweiler, G.R., Kouznetsova, T.B. et al. (2015). A coumarin dimer probe of mechanochemical scission efficiency in the sonochemical activation of chain-centered mechanophore polymers. *Chem. Commun.* 51 (44): 9157–9160.

61 Saitta, A.M., Soper, P.D., Wasserman, E., and Klein, M.L. (1999). Influence of a knot on the strength of a polymer strand. *Nature* 399 (6731): 46–48.

62 Stauch, T. and Dreuw, A. (2016). Knots "choke off" polymers upon stretching. *Angew. Chem. Int. Ed.* 55 (2): 811–814.

63 Patil, V.P., Sandt, J.D., Kolle, M., and Dunkel, J. (2020). Topological mechanics of knots and tangles. *Science* 367 (6473): 71–75.

64 Zhang, H., Chen, Y., Lin, Y. et al. (2014). Spiropyran as a mechanochromic probe in dual cross-linked elastomers. *Macromolecules* 47 (19): 6783–6790.

65 Celestine, A.D.N., Beiermann, B.A., May, P.A. et al. (2014). Fracture-induced activation in mechanophore-linked, rubber toughened PMMA. *Polymer (Guildf)* 55 (16): 4164–4171.

66 Clough, J.M., van der Gucht, J., Kodger, T.E., and Sprakel, J. (2020). Cephalopod-inspired high dynamic range mechano-imaging in polymeric materials. *Adv. Funct. Mater.* 30 (38), 2002716.

67 Chen, Y., Joshua Yeh, C., Qi, Y. et al. (2020). From force-responsive molecules to quantifying and mapping stresses in soft materials. *Sci. Adv.* 6 (20): 1–9.

68 Matsuda, T., Kawakami, R., Namba, R. et al. (2019). Mechanoresponsive self-growing hydrogels inspired by muscle training. *Science* 363 (6426): 504–508.

69 Shi, Z., Wu, J., Song, Q. et al. (2020). Toward drug release using polymer mechanochemical disulfide scission. *J. Am. Chem. Soc.* 142 (34): 14725–14732.

70 Huo, S., Zhao, P., Shi, Z. et al. (2021). Mechanochemical bond scission for the activation of drugs. *Nat. Chem.* 13 (2): 131–139.

71 Klein, I.M., Husic, C.C., Kovács, D.P. et al. (2020). Validation of the CoGEF method as a predictive tool for polymer mechanochemistry. *J. Am. Chem. Soc.* 142 (38): 16364–16381.

72 Davis, D.A., Hamilton, A., Yang, J. et al. (2009). Force-induced activation of covalent bonds in mechanoresponsive polymeric materials. *Nature* 459 (7243): 68–72.

73 Potisek, S.L., Davis, D.A., Sottos, N.R. et al. (2007). Mechanophore-linked addition polymers. *J. Am. Chem. Soc.* 129 (45): 13808–13809.

74 Kingsbury, C.M., May, P.A., Davis, D.A. et al. (2011). Shear activation of mechanophore-crosslinked polymers. *J. Mater. Chem.* 21 (23): 8381–8388.

75 Gossweiler, G.R., Hewage, G.B., Soriano, G. et al. (2014). Mechanochemical activation of covalent bonds in polymers with full and repeatable macroscopic shape recovery. *ACS Macro Lett.* 3 (3): 216–219.

76 Degen, C.M., May, P.A., Moore, J.S. et al. (2013). Time-dependent mechanochemical response of SP-cross-linked PMMA. *Macromolecules* 46 (22): 8917–8921.

77 Gossweiler, G.R., Kouznetsova, T.B., and Craig, S.L. (2015). Force-rate characterization of two spiropyran-based molecular force probes. *J. Am. Chem. Soc.* 137 (19): 6148–6151.

78 Beiermann, B.A., Davis, D.A., Kramer, S.L.B. et al. (2011). Environmental effects on mechanochemical activation of spiropyran in linear PMMA. *J. Mater. Chem.* 21 (23): 8443–8447.

79 Barbee, M.H., Kouznetsova, T., Barrett, S.L. et al. (2018). Substituent effects and mechanism in a mechanochemical reaction. *J. Am. Chem. Soc.* 140 (40): 12746–12750.

80 Zhang, H., Gao, F., Cao, X. et al. (2016). Mechanochromism and mechanical-force-triggered cross-linking from a single reactive moiety incorporated into polymer chains. *Angew. Chem. Int. Ed.* 55 (9): 3040–3044.

81 Versaw, B.A., McFadden, M.E., Husic, C.C., and Robb, M.J. (2020). Designing naphthopyran mechanophores with tunable mechanochromic behavior. *Chem. Sci.* 11 (17): 4525–4530.

82 Qian, H., Purwanto, N.S., Ivanoff, D.G. et al. (2021). Fast, reversible mechanochromism of regioisomeric oxazine mechanophores: developing in situ responsive force probes for polymeric materials. *Chem* 7 (4): 1080–1091.

83 McFadden, M.E. and Robb, M.J. (2019). Force-dependent multicolor mechanochromism from a single mechanophore. *J. Am. Chem. Soc.* 141 (29): 11388–11392.

84 Song, Y.K., Lee, K.H., Hong, W.S. et al. (2012). Fluorescence sensing of microcracks based on cycloreversion of a dimeric anthracene moiety. *J. Mater. Chem.* 22 (4): 1380–1386.

85 Kabb, C.P., O, Bryan, C.S., Morley, C.D. et al. (2019). Anthracene-based mechanophores for compression-activated fluorescence in polymeric networks. *Chem. Sci.* 10 (33): 7702–7708.

86 Konda, S.S.M., Brantley, J.N., Varghese, B.T. et al. (2013). Molecular catch bonds and the anti-hammond effect in polymer mechanochemistry. *J. Am. Chem. Soc.* 135 (34): 12722–12729.

87 Peterson, G.I., Lee, J., and Choi, T.L. (2019). Multimechanophore graft polymers: mechanochemical reactions at backbone-arm junctions. *Macromolecules* 52 (24): 9561–9568.

88 Sulkanen, A.R., Sung, J., Robb, M.J. et al. (2019). Spatially selective and density-controlled activation of interfacial mechanophores. *J. Am. Chem. Soc.* 141 (9): 4080–4085.

89 Göstl, R. and Sijbesma, R.P. (2016). π-Extended anthracenes as sensitive probes for mechanical stress. *Chem. Sci.* 7 (1): 370–375.

90 Li, J., Shiraki, T., Hu, B. et al. (2014). Mechanophore activation at heterointerfaces. *J. Am. Chem. Soc.* 136 (45): 15925–15928.

91 Li, J., Hu, B., Yang, K. et al. (2016). Effect of polymer grafting density on mechanophore activation at heterointerfaces. *ACS Macro Lett.* 5 (7): 819–822.

92 Stratigaki, M., Baumann, C., Van Breemen, L.C.A. et al. (2020). Fractography of poly(*N*-isopropylacrylamide) hydrogel networks crosslinked with mechanofluorophores using confocal laser scanning microscopy. *Polym. Chem.* 11 (2): 358–366.

93 Larsen, M.B. and Boydston, A.J. (2013). "Flex-activated" mechanophores: using polymer mechanochemistry to direct bond bending activation. *J. Am. Chem. Soc.* 135 (22): 8189–8192.

94 Larsen, M.B. and Boydston, A.J. (2014). Successive mechanochemical activation and small molecule release in an elastomeric material. *J. Am. Chem. Soc.* 136 (4): 1276–1279.

95 Hu, X., Zeng, T., Husic, C.C., and Robb, M.J. (2019). Mechanically triggered small molecule release from a masked furfuryl carbonate. *J. Am. Chem. Soc.* 141 (38): 15018–15023.

96 Akbulatov, S., Tian, Y., Huang, Z. et al. (2017). Experimentally realized mechanochemistry distinct from force-accelerated scission of loaded bonds. *Science* 357 (6348): 299–303.

97 Wang, J., Kouznetsova, T.B., Boulatov, R., and Craig, S.L. (2016). Mechanical gating of a mechanochemical reaction cascade. *Nat. Commun.* 7: 13433.

98 Hu, X., McFadden, M.E., Barber, R.W., and Robb, M.J. (2018). Mechanochemical regulation of a photochemical reaction. *J. Am. Chem. Soc.* 140 (43): 14073–14077.

99 Hsu, T.G., Zhou, J., Su, H.W. et al. (2020). A polymer with "locked" degradability: superior backbone stability and accessible degradability enabled by mechanophore installation. *J. Am. Chem. Soc.* 142 (5): 2100–2104.

100 Lin, Y., Kouznetsova, T.B., and Craig, S.L. (2020). Mechanically gated degradable polymers. *J. Am. Chem. Soc.* 142 (5): 2105–2109.

101 Barbee, M.H., Wang, J., Kouznetsova, T. et al. (2019). Mechanochemical ring-opening of allylic epoxides. *Macromolecules* 52 (16): 6234–6240.

102 Chen, Z., Mercer, J.A.M., Zhu, X. et al. (2017). Mechanochemical unzipping of insulating polyladderene to semiconducting polyacetylene. *Science* 357 (6350): 475–479.

103 Boswell, B.R., Mansson, C.M.F., Cox, J.M. et al. (2021). Mechanochemical synthesis of an elusive fluorinated polyacetylene. *Nat. Chem.* 13 (1): 41–46.

104 Mercer, J.A.M., Cohen, C.M., Shuken, S.R. et al. (2016). Chemical synthesis and self-assembly of a ladderane phospholipid. *J. Am. Chem. Soc.* 138 (49): 15845–15848.

105 Yang, J., Horst, M., Romaniuk, J.A.H. et al. (2019). Benzoladderene mechanophores: synthesis, polymerization, and mechanochemical transformation. *J. Am. Chem. Soc.* 141 (16): 6479–6483.

106 Yang, J., Horst, M., Werby, S.H. et al. (2020). Bicyclohexene- peri-naphthalenes: scalable synthesis, diverse functionalization, efficient polymerization, and facile mechanoactivation of their polymers. *J. Am. Chem. Soc.* 142 (34): 14619–14626.

107 Wang, F., Burck, M., and Diesendruck, C.E. (2017). Following homolytic mechanochemical kinetics with a pyrenyl nitrone spin trap. *ACS Macro Lett.* 6 (1): 42–45.

108 Ghosh, B. and Urban, M.W. (2009). Self-repairing oxetane-substituted chitosan polyurethane networks. *Science* 323: 1458–1460.

109 Amamoto, Y., Akamada, A., Otsuka, H. et al. (2011). Repeatable photoinduced self-healing of covalently cross-linked polymers through reshuffling of trithiocarbonate units. *Angew. Chem. Int. Ed.* 50: 1660–1663.

110 Yuan, C., Zhi Rong, M., Qiu Zhang, M. et al. (2011). Self-healing of polymers via synchronous covalent bond fission/radical recombination. *Chem. Mater.* 23 (22): 5076–5081.

111 Imato, K., Nishihara, M., Kanehara, T. et al. (2012). Self-healing of chemical gels cross-linked by diarylbibenzofuranone-based trigger-free dynamic covalent bonds at room temperature. *Angew. Chem.Int. Ed.* 51 (5): 1138–1142.

112 Frenette, M., Aliaga, C., Font-Sanchis, E., and Scaiano, J.C. (2004). Bond dissociation energies for radical dimers derived from highly stabilized carbon-centered radicals. *Org. Lett.* 6 (15): 2579–2582.

113 Imato, K., Kanehara, T., Ohishi, T. et al. (2015). Mechanochromic dynamic covalent elastomers: quantitative stress evaluation and autonomous recovery. *ACS Macro Lett.* 4 (11): 1307–1311.

114 Sumi, T., Goseki, R., and Otsuka, H. (2017). Tetraarylsuccinonitriles as mechanochromophores to generate highly stable luminescent carbon-centered radicals. *Chem. Commun.* 53 (87): 11885–11888.

115 Ishizuki, K., Oka, H., Aoki, D. et al. (2018). Mechanochromic polymers that turn green upon the dissociation of diarylbibenzothiophenonyl: the missing piece toward rainbow mechanochromism. *Chem. Eur. J.* 24 (13): 3170–3173.

116 Mori, Y., Yamada, N., Kanazawa, M. et al. (1996). Radical dissociation of 2,2′-bis(2-aryl-3-benzothiophenonyl)s by mechanical energy. *Bull. Chem. Soc. Jpn.* 69 (8): 2355–2359.

117 Sakai, H., Sumi, T., Aoki, D. et al. (2018). Thermally stable radical-type mechanochromic polymers based on difluorenylsuccinonitrile. *ACS Macro Lett.* 7 (11): 1359–1363.

118 Verstraeten, F., Göstl, R., and Sijbesma, R.P. (2016). Stress-induced colouration and crosslinking of polymeric materials by mechanochemical formation of triphenylimidazolyl radicals. *Chem. Commun.* 52 (55): 8608–8611.

119 Wu, Q., Yuan, Y., Chen, F. et al. (2020). Diselenide-linked polymers under sonication. *ACS Macro Lett.* 9 (11): 1547–1551.

120 Xia, J., Zhao, P., Pan, S., and Xu, H. (2019). Diselenide-containing polymeric vesicles with osmotic pressure response. *ACS Macro Lett.* 8 (6): 629–633.

121 Wang, Z., Ma, Z., Wang, Y. et al. (2015). A novel mechanochromic and photochromic polymer film: when rhodamine joins polyurethane. *Adv. Mater.* 27 (41): 6469–6474.

122 Karman, M., Verde-Sesto, E., and Weder, C. (2018). Mechanochemical activation of polymer-embedded photoluminescent benzoxazole moieties. *ACS Macro Lett.* 7 (8): 1028–1033.

123 Chen, Y., Spiering, A.J.H., Karthikeyan, S. et al. (2012). Mechanically induced chemiluminescence from polymers incorporating a 1,2-dioxetane unit in the main chain. *Nat. Chem.* 4 (7): 559–562.

124 Yang, F., Yuan, Y., Sijbesma, R.P., and Chen, Y. (2020). Sensitized mechanoluminescence design toward mechanically induced intense red emission from transparent polymer films. *Macromolecules* 53 (3): 905–912.

125 Ducrot, E., Chen, Y., Bulters, M. et al. (2014). Toughening elastomers with sacrificial bonds and watching them break. *Science* 344 (6180): 186–189.

126 Encina, M.V., Lissi, E., Sarasua, M. et al. (1980). Ultrasonic degradation of polyvinylpyrrolidone: effect of peroxide linkages. *J. Polym. Sci.: Polym. Lett. Ed.* 18 (12): 757–760.

127 Lin, Y., Barbee, M.H., Chang, C.-C., and Craig, S.L. (2018). Regiochemical effects on mechanophore activation in bulk materials. *J. Am. Chem. Soc.* 140 (46): 15969–15975.

128 Huheey, J. and Cottrell, T. (1958). *The Strengths of Chemical Bonds*. Waltham, MA: Butterworths.

129 Kersey, F.R., Yount, W.C., and Craig, S.L. (2006). Single-molecule force spectroscopy of bimolecular reactions: system homology in the mechanical activation of ligand substitution reactions. *J. Am. Chem. Soc.* 128 (12): 3886–3887.

130 Rodgers, M.T. and Armentrout, P.B. (2000). Noncovalent metal–ligand bond energies as studied by threshold collision-induced dissociation. *Mass Spectrom. Rev.* 19 (4): 215–247.

131 Skinner, H.A. and Connor, J.A. (1985). Metal–ligand bond-energies in organometallic compounds. *Pure Appl. Chem.* 57 (1): 79–88.

132 Sha, Y., Zhang, Y., Xu, E. et al. (2018). Quantitative and mechanistic mechanochemistry in ferrocene dissociation. *ACS Macro Lett.* 7 (10): 1174–1179.

133 Di Giannantonio, M., Ayer, M.A., Verde-Sesto, E. et al. (2018). Triggered metal ion release and oxidation: ferrocene as a mechanophore in polymers. *Angew. Chem. Int. Ed.* 57 (35): 11445–11450.

134 Zhang, Y., Wang, Z., Kouznetsova, T.B. et al. (2021). Distal conformational locks on ferrocene mechanophores guide reaction pathways for increased mechanochemical reactivity. *Nat. Chem.* 13 (1): 56–62.

135 Monsaert, S., Vila, A.L., Drozdzak, R. et al. (2009). Latent olefin metathesis catalysts. *Chem. Soc. Rev.* 38 (12): 3360–3372.

136 Piermattei, A., Karthikeyan, S., and Sijbesma, R.P. (2009). Activating catalysts with mechanical force. *Nat. Chem.* 1 (2): 133–137.

137 Ledoux, N., Allaert, B., Linden, A. et al. (2007). Bis-coordination of *N*-(alkyl)-*N*′-(2,6-diisopropylphenyl) heterocyclic carbenes to grubbs catalysts. *Organometallics* 26 (4): 1052–1056.

138 Ulman, M. and Grubbs, R.H. (1999). Ruthenium carbene-based olefin metathesis initiators: catalyst decomposition and longevity. *J. Org. Chem.* 64 (19): 7202–7207.

139 Küng, R., Pausch, T., Rasch, D. et al. (2021). Mechanochemical release of non-covalently bound guests from a polymer-decorated supramolecular cage. *Angew. Chem. Int. Ed.* 60 (24): 13626–13630.

140 Li, C.-H., Wang, C., Keplinger, C. et al. (2016). A highly stretchable autonomous self-healing elastomer. *Nat. Chem.* 8 (6): 618–624.

141 Brown, I.D. (2009). Recent developments in the methods and applications of the bond valence model. *Chem. Rev.* 109 (12): 6858–6919.

142 Yan, T., Schröter, K., Herbst, F. et al. (2017). What controls the structure and the linear and nonlinear rheological properties of dense, dynamic supramolecular polymer networks? *Macromolecules* 50 (7): 2973–2985.

143 Zhang, Q., Zhu, X., Li, C.-H. et al. (2019). Disassociation and reformation under strain in polymer with dynamic metal–ligand coordination cross-linking. *Macromolecules* 52 (2): 660–668.

144 Chen, Y., Kushner, A.M., Williams, G.A., and Guan, Z. (2012). Multiphase design of autonomic self-healing thermoplastic elastomers. *Nat. Chem.* 4 (6): 467.

145 Zhao, P.-C., Li, W., Huang, W., and Li, C.-H. (2020). A self-healing polymer with fast elastic recovery upon stretching. *Molecules* 25 (3): 597.

146 Kang, J., Son, D., Wang, G.N. et al. (2018). Tough and water-insensitive self-healing elastomer for robust electronic skin. *Adv. Mater.* 30 (13): 1706846.

147 Mozhdehi, D., Neal, J.A., Grindy, S.C. et al. (2016). Tuning dynamic mechanical response in metallopolymer networks through simultaneous control of structural and temporal properties of the networks. *Macromolecules* 49 (17): 6310–6321.

148 Sun, J.-Y., Zhao, X., Illeperuma, W.R.K. et al. (2012). Highly stretchable and tough hydrogels. *Nature* 489 (7414): 133–136.

149 Morelle, X.P., Illeperuma, W.R., Tian, K. et al. (2018). Highly stretchable and tough hydrogels below water freezing temperature. *Adv. Mater.* 30 (35): 1801541.

150 Guo, H., Han, Y., Zhao, W. et al. (2020). Universally autonomous self-healing elastomer with high stretchability. *Nat. Commun.* 11: 2037.

151 Urban, M.W., Davydovich, D., Yang, Y. et al. (2018). Key-and-lock commodity self-healing copolymers. *Science* 362 (6411): 220–225.

152 Wang, S. and Urban, M.W. (2020). Self-healing polymers. *Nat. Rev. Mater.* 5 (8): 562–583.

153 Yang, Y. and Urban, M.W. (2013). Self-healing polymeric materials. *Chem. Soc. Rev.* 42 (17): 7446–7467.

154 Zheng, N., Xu, Y., Zhao, Q., and Xie, T. (2021). Dynamic covalent polymer networks: a molecular platform for designing functions beyond chemical recycling and self-healing. *Chem. Rev.* 121 (3): 1716–1745.

155 Roy, N., Bruchmann, B., and Lehn, J.M. (2015). DYNAMERS: dynamic polymers as self-healing materials. *Chem. Soc. Rev.* 44 (11): 3786–3807.

156 Wojtecki, R.J., Meador, M.A., and Rowan, S.J. (2011). Using the dynamic bond to access macroscopically responsive structurally dynamic polymers. *Nat. Mater.* 10 (1): 14–27.

157 Zhao, P., Huo, S., Fan, J. et al. (2021). Activation of the catalytic activity of thrombin for fibrin formation by ultrasound. *Angew. Chem. Int. Ed.* 60 (26): 14707–14714.

158 Zhang, M., Xu, D., Yan, X. et al. (2012). Self-healing supramolecular gels formed by crown ether based host–guest interactions. *Angew. Chem.* 124 (28): 7117–7121.

159 Miyamae, K., Nakahata, M., Takashima, Y., and Harada, A. (2015). Self-healing, expansion–contraction, and shape-memory properties of a preorganized supramolecular hydrogel through host–guest interactions. *Angew. Chem. Int. Ed.* 54 (31): 8984–8987.

160 Hippler, M., Weißenbruch, K., Richler, K. et al. (2020). Mechanical stimulation of single cells by reversible host–guest interactions in 3D microscaffolds. *Sci. Adv.* 6 (39): eabc2648.

161 Sugawara, A., Asoh, T.-A., Takashima, Y. et al. (2021). Mechano-responsive hydrogels driven by the dissociation of a host–guest complex. *ACS Macro Lett.* 10 (7): 971–977.

162 Bhangu, S.K., Bocchinfuso, G., Ashokkumar, M., and Cavalieri, F. (2020). Sound-driven dissipative self-assembly of aromatic biomolecules into functional nanoparticles. *Nanoscale Horiz.* 5 (3): 553–563.

163 Self, J.L., Sample, C.S., Levi, A.E. et al. (2020). Dynamic bottlebrush polymer networks: self-healing in super-soft materials. *J. Am. Chem. Soc.* 142 (16): 7567–7573.

164 Jo, Y.H., Li, S., Zuo, C. et al. (2020). Self-healing solid polymer electrolyte facilitated by a dynamic cross-linked polymer matrix for lithium–ion batteries. *Macromolecules* 53 (3): 1024–1032.

165 Pan, Y., Zhang, H., Xu, P. et al. (2020). A mechanochemical reaction cascade for controlling load-strengthening of a mechanochromic polymer. *Angew. Chem. Int. Ed.* 59 (49): 21980–21985.

166 Wang, Z., Wang, J., Ayarza, J. et al. (2021). Bio-inspired mechanically adaptive materials through vibration-induced crosslinking. *Nat. Mater.* 20: 869–874.

167 Gao, Q., Kopera, B.A.F., Zhu, J. et al. (2020). Breathable and flexible polymer membranes with mechanoresponsive electric resistance. *Adv. Funct. Mater.* 30 (26): 1907555.

168 Ashizawa, M., Zheng, Y., Tran, H., and Bao, Z. (2020). Intrinsically stretchable conjugated polymer semiconductors in field effect transistors. *Prog. Polym. Sci.* 100: 101181.

169 Yao, B., Hong, W., Chen, T. et al. (2020). Highly stretchable polymer composite with strain-enhanced electromagnetic interference shielding effectiveness. *Adv. Mater.* 32 (14): 1907499.

170 Kim, D.C., Shim, H.J., Lee, W. et al. (2020). Material-based approaches for the fabrication of stretchable electronics. *Adv. Mater.* 32 (15): 1902743.